OPEN ACCESS

University of BRISTOL

Peer reviewed version

License (if available):
CC BY-NC

Link to published version (if available):
10.1002/rnc.3878

Link to publication record in Explore Bristol Research
PDF-document

University of Bristol - Explore Bristol Research
General rights

Aeroelastic modeling and stability analysis:
a robust approach to the flutter problem

Andrea Iannelli*, Andrés Marcos, Mark Lowenberg

Department of Aerospace Engineering, University of Bristol, BS8 1TR, United Kingdom

SUMMARY

In this paper a general approach to address modeling of aeroelastic systems, with the final goal to apply μ analysis, is discussed. The chosen test bed is the typical section with unsteady aerodynamic loads, which enables basic modeling features to be captured and so extend the gained knowledge to practical problems treated with modern techniques. The aerodynamic operator has a non-rational dependence on the Laplace variable s and hence two formulations for the problem are available: frequency domain or state-space (adopting rational approximations). The study attempts to draw a parallel between the two consequent LFT modeling processes, emphasizing critical differences and their effect on the predictions obtained with μ analysis. A peculiarity of this twofold formulation is that aerodynamic uncertainties are inherently treated differently and therefore the families of plants originated by the possible LFT definitions are investigated. One of the main results of the paper is to propose a unified framework to address the robust modeling task, which enables the advantages of both the approaches to be retained. On the analysis side, the application of μ analysis to the different models is shown, emphasizing its capability to gain insight into the problem. Copyright © 2017 John Wiley & Sons, Ltd.

1. INTRODUCTION

Flutter is a self-excited instability in which aerodynamic forces on a flexible body couple with its natural vibration modes producing oscillatory motion. The level of vibration may result in sufficiently large amplitudes to provoke failure and often this phenomenon dictates the design of the aerodynamic body. Thus, flutter analysis has been widely investigated and there are several techniques representing the state-of-practice [1]. The major methods are based on the frequency domain as this is the framework in which the aerodynamic loads are more often expressed for stability analysis.

---

*Correspondence to: Andrea Iannelli, University of Bristol, BS8 1TR, United Kingdom. Email: andrea.iannelli@bristol.ac.uk

Despite the large amount of effort spent in understanding flutter, it is acknowledged that predictions based only on computational analyses are not totally reliable [2]. Currently this is compensated by the addition of conservative safety margins to the analysis results and expensive flutter test campaigns. One of the main criticalities in flutter analysis arises from the sensitivity of aeroelastic instability to small variations in parameter and modeling assumptions. In addressing this issue, in the last decade researchers looked at robust modeling and analysis techniques from the robust control community, specifically Linear Fractional Transformation (LFT) models and structured singular value (s.s.v.) analysis [3, 4]. The so-called flutter robust analysis aims to quantify the gap between the prediction of the nominal stability analysis (model without uncertainties) and the worst-case scenario when the whole set of uncertainty is contemplated. The most well-known robust flutter approaches are those from [5], [6], [7], with the first even demonstrating on-line analysis capabilities during flight tests [8].

Each of the aforementioned robust flutter approaches used the same underlying μ analysis tools but a different LFT model development path. The goal of each of those robust flutter studies was to provide an end-to-end process, from robust modeling to analysis, and demonstrate the validity of the approach. Since this was their focus, no detailed study or comparison was performed on the effect the modeling choices have on the analysis, although it is well-known in the robust control community that this is a fundamental issue [9, 10, 11].

One of the goals of this article, which builds on the initial work contained in [12], is thus to present a review of the robust modeling options available for aeroelastic systems, providing also a better understanding of their effects on the analyses. A second goal is to provide a basis for communication between the robust control and the aeroelastic communities by reconciling and detailing the analyses performed from both perspectives.

In this article it will be shown that the main differences in the definition of the aeroelastic plant arise due to the unsteady aerodynamic operator which has a non-rational dependence on the Laplace variable s. This allows formulation of the problem following two distinct paths: the frequency domain and the state-space (which includes rational approximations for the aerodynamic operator). A systematic comparison between these two approaches is addressed, highlighting critical aspects. An important feature is that the uncertainty description of the aerodynamic part of the system is closely connected with the LFT approach adopted. Strengths and weaknesses of the two formulations are discussed, and finally a unified approach having the main advantages from each path is proposed and validated against the *typical section* test bed. In aeroelastic jargon this name commonly refers to a simplified model describing a characteristic section of the wing [13].

In addition, illustrative applications of robust flutter analysis within the s.s.v. framework are presented. On the one hand they show the results obtained with different LFT models, and on the other they stress the various types of information that can be inferred from μ analysis.

The layout of the article is as follows. Section 2 provides a cursory introduction to the techniques employed in the work. Section 3 presents the main aspects of the nominal aeroelastic modeling applied to the typical section test bed, including a description of the algorithms employed for the aerodynamics rational approximations. Section 4 gathers the main results of the paper, and is dedicated to the LFT modeling process and the aerodynamic uncertainty characterization. Finally, the robust predictions obtained applying μ analysis to the presented framework are illustrated in Section 5.

2. THEORETICAL BACKGROUND

This section provides the reader with the essential notions related to LFT [3] and μ analysis [4]. The first is an instrumental framework in modern control theory for robustness analysis and synthesis. The underpinning idea is to represent an uncertain system in terms of nominal and uncertain components given by matrices. Its prowess in addressing the modeling of complex uncertain systems has been extensively demonstrated in the last decades, with particular emphasis on aerospace applications, providing: models for the analysis of the flight control system for the X-38 crew return vehicle [14]; Linear-Parameter-Varying (LPV) models for the Boeing 747 [9]; and reduced order models for flexible aircraft [15].

The structured singular value enables the robust stability and performance of a system subject to real parametric and dynamic uncertainties to be addressed. Examples of successful applications are: robustness assessment of an $\mathcal{H}_\infty$ controller for a missile autopilot in the face of large real parametric aerodynamic uncertainties [16]; identification of the worst-case uncertain parameter combinations for the lateral-axis dynamics of a generic civil transport aircraft [17]; control law assessment for the Vega launcher thrust vector control system [18].

As for the notation, common definitions are adopted. $\mathbb{C}^{n \times m}$ denotes complex valued matrices with n rows and m columns. Given a matrix P, $\sigma(P)$ indicated the singular values of P and $\bar{\sigma}(P)$ the maximum singular value. The asterisk $*$ will be used for component-wise product between vectors. In the text, matrices and vectors are indicated with bold characters. Inside the equations, matrices are enclosed in square brackets to differentiate them from vectors when there is ambiguity.

2.1. Linear Fractional Transformation

Let $\mathbf{M}$ be a complex *coefficient matrix* partitioned as:

$$\begin{bmatrix} \mathbf{M} \end{bmatrix} = \begin{bmatrix} \mathbf{M_{11}} & \mathbf{M_{12}} \\ \mathbf{M_{21}} & \mathbf{M_{22}} \end{bmatrix} \in \mathbb{C}^{(p_1+p_2)\times(q_1+q_2)} \tag{1}$$

and let $\mathbf{\Delta_l} \in \mathbb{C}^{q_2 \times p_2}$ and $\mathbf{\Delta_u} \in \mathbb{C}^{q_1 \times p_1}$. The lower LFT with respect to $\mathbf{\Delta_l}$ is defined as the map:

$$\mathcal{F}_l(\mathbf{M}, \bullet) : \mathbb{C}^{q_2 \times p_2} \longrightarrow \mathbb{C}^{p_1 \times q_1}$$
$$\mathcal{F}_l(\mathbf{M}, \mathbf{\Delta_l}) = \mathbf{M_{11}} + \mathbf{M_{12}}\mathbf{\Delta_l}(\mathbf{I} - \mathbf{M_{22}}\mathbf{\Delta_l})^{-1}\mathbf{M_{21}} \tag{2}$$

Similarly the upper LFT with respect to $\mathbf{\Delta_u}$ is defined as the map:

$$\mathcal{F}_u(\mathbf{M}, \bullet) : \mathbb{C}^{q_1 \times p_1} \longrightarrow \mathbb{C}^{p_2 \times q_2}$$
$$\mathcal{F}_u(\mathbf{M}, \mathbf{\Delta_u}) = \mathbf{M_{22}} + \mathbf{M_{21}}\mathbf{\Delta_u}(\mathbf{I} - \mathbf{M_{11}}\mathbf{\Delta_u})^{-1}\mathbf{M_{12}} \tag{3}$$

The terminology is motivated by the feedback representation usually adopted to depict an LFT, see Figure 1. Each map is associated with a set of equations, where $\mathbf{y}$ can be interpreted as an output of the system when $\mathbf{u}$ is applied, while $\mathbf{w}$ and $\mathbf{z}$ are signals closing the feedback loop. If the relation between $\mathbf{u}$ and $\mathbf{y}$ is sought, the expressions in (2)-(3) are obtained. Both expressions are equivalent. In this work $\mathcal{F}_u$ is meant to be adopted, except where explicitly noted, and thus the related subscript u is dropped.
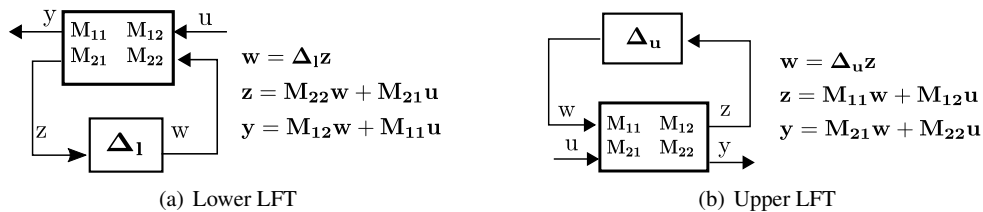
Figure 1. Linear Fractional Transformation (LFT)

Looking at (3) and Figure 1(b), an interpretation of the upper LFT can be inferred. If $\mathbf{M}$ is taken as a proper transfer matrix, $\mathcal{F}_u$ is the closed-loop transfer matrix from input $\mathbf{u}$ to output $\mathbf{y}$ when the nominal plant $\mathbf{M_{22}}$ is subject to a perturbation matrix $\boldsymbol{\Delta}$. The matrices $\mathbf{M_{11}}$, $\mathbf{M_{12}}$ and $\mathbf{M_{21}}$ reflect a priori knowledge of how the perturbation affects the nominal map. Once all varying or uncertain parameters are *pulled out* of the nominal plant, the problem appears as a nominal system subject to an artificial feedback. A crucial feature apparent in (3) is that the LFT is well posed if and only if the inverse of $(\mathbf{I} - \mathbf{M_{11}}\boldsymbol{\Delta})$ exists, where $\mathbf{M_{11}}$ is by definition the transfer matrix seen by the perturbation block $\boldsymbol{\Delta}$.

It is remarked here that many types of dynamical systems can be recast as LFTs, including those represented by multivariate polynomial matrices (e.g. all those described by Ordinary Differential Equations). Moreover, for these a lower order representation can be achieved [19, 20].

2.2. μ analysis

The structured singular value is a matrix function denoted by $\mu_{\boldsymbol{\Delta}}(\mathbf{M})$, where $\boldsymbol{\Delta}$ is a structured uncertainty set. The mathematical definition follows:

$$\mu_{\boldsymbol{\Delta}}(\mathbf{M}) = \left(\min_{\hat{\boldsymbol{\Delta}} \in \boldsymbol{\Delta}} \left(\bar{\sigma}(\hat{\boldsymbol{\Delta}}) : \det(\mathbf{I} - \mathbf{M}\hat{\boldsymbol{\Delta}}) = 0 \right) \right)^{-1} \tag{4}$$

if $\exists \hat{\boldsymbol{\Delta}} \in \boldsymbol{\Delta}$ such that $\det(\mathbf{I} - \mathbf{M}\hat{\boldsymbol{\Delta}}) = 0$ and otherwise $\mu_{\boldsymbol{\Delta}}(\mathbf{M}) := 0$.

Equation (4) can then be specialized to the study of the robust stability (RS) of the plant represented by $\mathcal{F}_u(\mathbf{M}, \boldsymbol{\Delta})$. At a fixed frequency ω, the *coefficient matrix* $\mathbf{M}$ is a complex valued matrix; in particular $\mathbf{M_{11}}$ is known, which is the transfer matrix from the signal $\mathbf{w}$ to $\mathbf{z}$. The RS problem can then be formulated as a μ calculation:

$$\mu_{\boldsymbol{\Delta}}(\mathbf{M_{11}}) = \left(\min_{\hat{\boldsymbol{\Delta}} \in \boldsymbol{\Delta}} (\hat{\beta} : \det(\mathbf{I} - \hat{\beta}\mathbf{M_{11}}\hat{\boldsymbol{\Delta}}) = 0; \quad \bar{\sigma}(\hat{\boldsymbol{\Delta}}) \leq 1) \right)^{-1} \tag{5}$$

where $\hat{\beta}$ is a real positive scalar and $\boldsymbol{\Delta}$ is the uncertainty set associated with $\mathcal{F}_u(\mathbf{M}, \boldsymbol{\Delta})$. For ease of calculation and interpretation, this set is norm-bounded (i.e. $\bar{\sigma}(\boldsymbol{\Delta}) \leq 1$) by scaling of $\mathbf{M_{11}}$ without loss of generality. The result can then be interpreted as follows: if $\mu_{\boldsymbol{\Delta}}(\mathbf{M_{11}}) \leq 1$ then there is no perturbation matrix inside the allowable set $\boldsymbol{\Delta}$ such that the determinant condition is satisfied, that is $\mathcal{F}_u(\mathbf{M}, \boldsymbol{\Delta})$ is well posed and thus the associated plant is robust stable within the range of uncertainties considered. On the contrary, if $\mu_{\boldsymbol{\Delta}}(\mathbf{M_{11}}) \geq 1$ a candidate (that is belonging to the allowed set) perturbation matrix exists which violates the well-posedness, i.e. the closed loop in Figure 1(b) is unstable. In particular, the reciprocal of μ (auxiliary notation is dropped for clarity) provides directly a measure (i.e. its $\|\cdot\|_\infty$ norm $\hat{\beta}$) of the smallest structured uncertainty matrix that

causes instability. The s.s.v. can also be used as a robust performance (RP) test. In that case, the full *coefficient matrix* $\mathbf{M}$ is employed in the calculation.

It is known that $\mu_{\mathbf{\Delta}}(\mathbf{M})$ is NP-hard with either pure real or mixed real-complex uncertainties [21], except for a few special cases, thus all μ algorithms work by searching for upper and lower bounds.

The upper bound μ_{UB} provides the maximum size perturbation $\|\mathbf{\Delta}_{UB}\|_\infty = 1/\mu_{UB}$ for which RS is guaranteed, whereas the lower bound μ_{LB} defines a minimum size perturbation $\|\mathbf{\Delta}_{LB}\|_\infty = 1/\mu_{LB}$ for which RS is guaranteed to be violated. If the bounds are close in magnitude then the conservativeness in the calculation of μ is small, otherwise nothing can be said on the guaranteed robustness of the system for perturbations within $[1/\mu_{UB}, 1/\mu_{LB}]$. Along with this information, the lower bound also provides the matrix $\mathbf{\Delta}_{LB} = \mathbf{\Delta}^{cr}$ satisfying the determinant condition.

3. AEROELASTIC MODEL

The *typical section* model was introduced in the early stages of the establishment of the aeroelasticity field in order to investigate dynamic phenomena such as flutter [13]. Its validity was assessed to quantitatively study the dynamics of an unswept wing when the properties are taken at a station 70-75% from the centerline. Despite its simplicity, it captures essential effects in a simple model representation, see Figure 2.

Figure 2. Typical section sketch

From the structural side, it basically consists of a rigid airfoil with lumped springs simulating the 3 degrees of freedom (DOFs) of the section: plunge h, pitch α and trailing edge flap β. The positions of the elastic axis (EA), center of gravity (CG) and the aerodynamic center (AC) are also marked. The main parameters in the model are: K_h, K_α and K_β –respectively the bending, torsional and control surface stiffness; half chord distance b; dimensionless distances a, c from the mid-chord to the flexural axis and the hinge location respectively, and x_α and x_β, which are dimensionless distances from flexural axis to airfoil center of gravity and from hinge location to control surface center of gravity.

In addition to the above parameters, the inertial characteristics of the system are given by: the wing mass per unit span m_s, the moment of inertia of the section about the elastic axis I_α, and the moment of inertia of the control surface about the hinge I_β. If structural damping is considered, this can be expressed specifying the damping ratios for each DOF and then applied as modal damping.

The most standard unsteady aerodynamic formulation is based on the Theodorsen approach [22]. This formulation is based on the assumption of a thin airfoil moving with small harmonic oscillations in a potential and incompressible flow.

In order to present the basic model development approach, $\mathbf{X}$ and $\mathbf{L_a}$ are defined as the vectors of the degrees of freedom and of the aerodynamic loads respectively:

$$\mathbf{X}(t) = \begin{bmatrix} \frac{h(t)}{b} \\ \alpha(t) \\ \beta(t) \end{bmatrix} ; \quad \mathbf{L_a}(t) = \begin{bmatrix} -L(t) \\ M_\alpha(t) \\ M_\beta(t) \end{bmatrix} \tag{6}$$

In addition, $\mathbf{M_s}$, $\mathbf{C_s}$ and $\mathbf{K_s}$ are respectively the structural mass, damping and stiffness matrices:

$$\mathbf{M_s} = m_s b^2 \begin{bmatrix} 1 & x_\alpha & x_\beta \\ x_\alpha & r_\alpha^2 & r_\beta^2 + x_\beta(c-a) \\ x_\beta & r_\beta^2 + x_\beta(c-a) & r_\beta^2 \end{bmatrix}$$

$$\mathbf{C_s} = \begin{bmatrix} c_h & 0 & 0 \\ 0 & c_\alpha & 0 \\ 0 & 0 & c_\beta \end{bmatrix} ; \quad \mathbf{K_s} = \begin{bmatrix} K_h & 0 & 0 \\ 0 & K_\alpha & 0 \\ 0 & 0 & K_\beta \end{bmatrix} \tag{7}$$

where $r_\alpha = \sqrt{\frac{I_\alpha}{m_s b^2}}$ and $r_\beta = \sqrt{\frac{I_\beta}{m_s b^2}}$ are respectively the dimensionless radius of gyration of the section and of the control surface. The values of the parameters for the studied test case are reported in Tab. II in Appendix A.

The set of differential equations describing the dynamic equilibrium can then be recast in matrix form using Lagrange's equations:

$$\big[\mathbf{M_s}\big]\ddot{\mathbf{X}} + \big[\mathbf{C_s}\big]\dot{\mathbf{X}} + \big[\mathbf{K_s}\big]\mathbf{X} = \mathbf{L_a} \tag{8}$$

The expression for the aeroelastic loads $\mathbf{L_a}$, provided in the Laplace s domain, is:

$$\mathbf{L_a}(s) = q\big[\mathbf{A}(\bar{s})\big]\mathbf{X}(s) \tag{9}$$

where the dynamic pressure q and the dimensionless Laplace variable $\bar{s}$ ($= s\frac{b}{V}$ with V the wind speed) are introduced. $\mathbf{A}(\bar{s})$ is called the generalized Aerodynamic Influence Coefficient (AIC) matrix, and is composed of generic terms A_{ij} representing the transfer function from each degree of freedom j in $\mathbf{X}$ to each aerodynamic load component i in $\mathbf{L_a}$. Due to the motion assumptions underlying Theodorsen theory, the expression in (9) has to be evaluated at $\bar{s} = i\frac{\omega b}{V} = ik$, where k is called the *reduced frequency* and plays a crucial role in flutter analyses. The AIC matrix expression is:

$$\mathbf{A}(\bar{s}) = S\bigg(\big[\mathbf{M_{nc}}\big]\bar{s}^2 + \big(\big[\mathbf{B_{nc}}\big] + C(\bar{s})\big[\mathbf{RS_1}\big]\big)\bar{s} + \big[\mathbf{K_{nc}}\big] + C(\bar{s})\big[\mathbf{RS_2}\big]\bigg) \tag{10}$$

where S is the wing surface, $C(\bar{s})$ is the Theodorsen function and $\mathbf{M_{nc}}$, $\mathbf{B_{nc}}$, $\mathbf{K_{nc}}$, $\mathbf{RS_1}$ and $\mathbf{RS_2}$ are real coefficients matrices (see Appendix A for details).

As aforementioned, despite its simplicity, such a description of the aerodynamic forces is pertinent to analyse flutter, which is defined as a condition of neutral stability of the system, i.e.

pure harmonic motion. This explains why this theory, although being generalized to an arbitrary airfoil motion, has represented a paradigm for more improved models aimed at flutter analysis. The most well-known aerodynamic solver in the field, named Doublet Lattice Method (DLM) and introduced in [23], operates always in the framework of potential theory and harmonic motion of the body and provides the same relation as in (9) between the elastic displacements of the structure and the aerodynamic loads acting on it.

Due to the expression of the AIC matrix which does not have a rational dependence on the Laplace variable s, the final aeroelastic equilibrium is inherently expressed in the frequency domain:

$$\left[\left[\mathbf{M_s}\right]s^2 + \left[\mathbf{C_s}\right]s + \left[\mathbf{K_s}\right]\right]\mathbf{X} = q\left[\mathbf{A}(\bar{s})\right]\mathbf{X} \tag{11}$$

Equation (11) represents therefore the starting point for current industrial state-of-practice analysis of linear flutter stability [24].

This subsection is concluded with an example of time-response of the three DOFs of the typical section: dimensionless plunge $\frac{h}{b}$, pitch rotation α and trailing edge flap rotation β. The simulation, obtained using one of the rational approximations later introduced for the aerodynamics loads, is generated imposing null initial conditions for the DOFs and their derivatives, except for the plunge displacement which is assigned an initial value of $\frac{h}{b}\big|_{t=0}$=0.05. The response of the system (refer to Figure 3) is observed at two different speeds, namely V=295 $\frac{m}{s}$ and V=307 $\frac{m}{s}$. Two remarkably different behaviors can be detected, with the former speed resulting in stable behavior and the latter unstable.
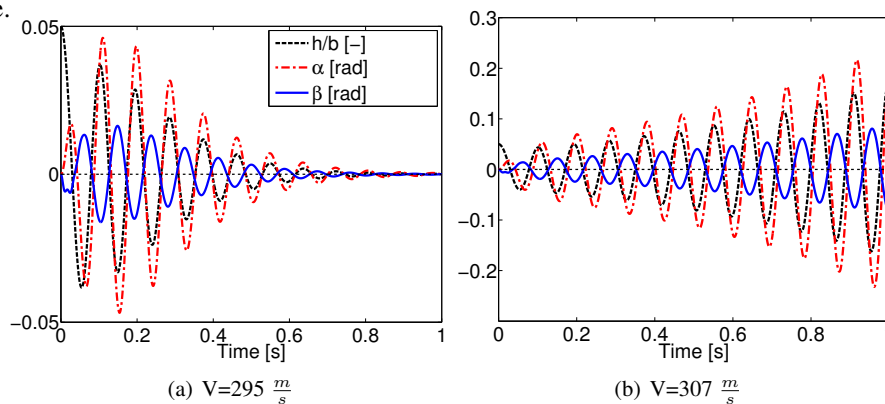

(a) V=295 $\frac{m}{s}$ (b) V=307 $\frac{m}{s}$

Figure 3. Time-responses of the typical section DOFs at two different speeds

3.1. Rational Approximations

Rational approximations of the AIC matrix are sought in order to provide an expression of (11) in state-space, which is generally required for application of either robust analysis or control design techniques.

The difference between a quasi-steady and an unsteady formulation of the aerodynamic loads is that the latter attempts to model the memory effect of the flow, which results in phase shift and magnitude change of the loads with respect to the former one. This is commonly referred to as *time lag* effect. A general two-part approximation model can then be obtained based on *quasi-steady* (QS) and *lag* contributions:

$$\mathbf{A}(\bar{s}) \approx \mathbf{\Gamma}_{QS} + \mathbf{\Gamma}_{lag} \tag{12}$$

In this paper two of the most established algorithms are considered: the Roger [25] and the Minimum State [26] methods. They propose a formally identical expression for $\mathbf{\Gamma}_{QS}$:

$$\mathbf{\Gamma}_{QS} = \left[\mathbf{A_2}\right]\bar{s}^2 + \left[\mathbf{A_1}\right]\bar{s} + \left[\mathbf{A_0}\right] \tag{13}$$

Where $\mathbf{A_2}$, $\mathbf{A_1}$ and $\mathbf{A_0}$ are real coefficient matrices modeling respectively the contribution of acceleration, speed and displacement of the elastic degrees of freedom on the load.

Roger proposed that $\mathbf{\Gamma}_{lag}$ could be approximated as:

$$\mathbf{\Gamma}_{lag-Rg} = \sum_{L=3}^{N} \frac{\bar{s}}{\bar{s} + \gamma_{L-2}} \left[\mathbf{A_L}\right] \tag{14}$$

The partial fractions inside the summation are the so-called *lag terms* and they basically represent high-pass filters with the aerodynamic roots γ_i, selected by the user, as cross-over frequencies. The real coefficient matrices $\mathbf{A_i}$ with $i = 0...N$, where N-2 is the number of lag terms, are found using a linear least-square technique for a term-by-term fitting of the aerodynamic operator. The resulting state-space equation includes augmented states $\hat{\mathbf{X}}_{\mathbf{aL}}$ representing the aerodynamic lags, which are equal to the number of roots multiplied by the number of degrees of freedom.

Once the AIC matrix is written as in (12) according to the Roger approximation, its expression is substituted in (11) and then it is possible to write the sought state-space form:

$$\begin{bmatrix} \dot{\mathbf{X}} \\ \ddot{\mathbf{X}} \\ \dot{\hat{\mathbf{X}}}_{\mathbf{a3}} \\ \vdots \\ \dot{\hat{\mathbf{X}}}_{\mathbf{aN}} \end{bmatrix} = \begin{bmatrix} 0 & \left[\mathbf{I}\right] & 0 & ... & 0 \\ -\left[\mathbf{M}\right]^{-1}\left[\mathbf{K}\right] & -\left[\mathbf{M}\right]^{-1}\left[\mathbf{B}\right] & q\left[\mathbf{M}\right]^{-1}\left[\mathbf{A_3}\right] & ... & q\left[\mathbf{M}\right]^{-1}\left[\mathbf{A_N}\right] \\ 0 & \left[\mathbf{I}\right] & -\frac{V}{b}\gamma_1\left[\mathbf{I}\right] & ... & 0 \\ \vdots & \vdots & \vdots & \ddots & \\ 0 & \left[\mathbf{I}\right] & 0 & & -\frac{V}{b}\gamma_{N-2}\left[\mathbf{I}\right] \end{bmatrix} \begin{bmatrix} \mathbf{X} \\ \dot{\mathbf{X}} \\ \hat{\mathbf{X}}_{\mathbf{a3}} \\ \vdots \\ \hat{\mathbf{X}}_{\mathbf{aN}} \end{bmatrix} \tag{15}$$

where:

$$\begin{align} \left[\mathbf{M}\right] &= \left[\mathbf{M}_s\right] - \frac{1}{2}\rho_\infty b^2\left[\mathbf{A_2}\right] \\ \left[\mathbf{B}\right] &= \left[\mathbf{C}_s\right] - \frac{1}{2}\rho_\infty bV\left[\mathbf{A_1}\right] \\ \left[\mathbf{K}\right] &= \left[\mathbf{K}_s\right] - \frac{1}{2}\rho_\infty V^2\left[\mathbf{A_0}\right] \end{align} \tag{16}$$

$\mathbf{M}$, $\mathbf{B}$ and $\mathbf{K}$ are respectively the aeroelastic inertial, damping and stiffness matrices. In fact they include the structural terms plus the aerodynamic quasi-steady contributions.

The Minimum State (MS) method tries to improve the efficiency of Roger's in terms of number of augmented states per given accuracy of the approximation. There is no clear quantification of this advantage, but it has been stated [27] that the number of aerodynamic states required by MS may typically be 6-8 times smaller than with the adoption of Roger method for the same level of model accuracy in realistic aeroelastic design (i.e. aircraft application). The MS $\mathbf{\Gamma}_{lag}$ expression is:

$$\mathbf{\Gamma}_{lag-MS} = \left[\mathbf{D}'\right] \begin{bmatrix} \frac{1}{\bar{s}+\gamma_1} & ... & 0 \\ \vdots & \ddots & \vdots \\ 0 & ... & \frac{1}{\bar{s}+\gamma_{N-2}} \end{bmatrix} \left[\mathbf{E}'\right]\bar{s} \tag{17}$$

The coefficients of $\left[\mathbf{D}'\right]$ and $\left[\mathbf{E}'\right]$ are iteratively determined through a nonlinear least square since (17) is bilinear in these two unknowns, while the matrices defining $\mathbf{\Gamma}_{QS}$ are obtained imposing the constraint of matching the aerodynamic operator at $k=0$ as well as at another reduced frequency k_c. The latter is usually selected close to the reduced flutter frequency. A possible strategy is to guess its value for the first flutter calculation and then update the rational approximation with the new value of k_c based on the predicted reduced flutter frequency. Note that the number of augmented states is now equal to the number of roots.

Equations (14)-(17) show the *formal* difference in the expression of $\mathbf{\Gamma}_{lag}$ for these approximations, and in particular in the role played by the aerodynamic roots γ_{i-2}. In Roger's method there is a one-to-one correspondence between the N-2 gains of the high-pass filters (generic term of $\mathbf{A_L}$) and their cross-over frequencies γ_{L-2}, whereas in the MS method there is a *coupling* between the various gains and roots as a consequence of the compact expression of $\mathbf{\Gamma}_{lag-MS}$. The impact that the differences in the expression of $\mathbf{\Gamma}_{lag}$ have on LFT modeling and robust analysis when lag terms are uncertain will be investigated respectively in Subsections 4.2 and 5.4.

Figure 4 shows the Bode plot of the aerodynamic transfer functions from plunge, pitch rotation and flap rotation to the pitch moment M_α. Five curves in each subplot are depicted, representing the different expressions of the aerodynamic operators introduced earlier: the Theodorsen operator $\mathbf{A}(\bar{s})$; Roger approximation considering separately quasi-steady and lag contributions (i.e. $\mathbf{\Gamma}_{QS-Rg}$ and $\mathbf{\Gamma}_{lag-Rg}$); Minimum State method (in analogy with Roger $\mathbf{\Gamma}_{QS-MS}$ and $\mathbf{\Gamma}_{lag-MS}$).

In conclusion, both the approximation algorithms lead to the same short-hand state matrix:

$$\begin{bmatrix} \dot{\hat{\mathbf{X}}}_{\mathbf{s}} \\ \dot{\hat{\mathbf{X}}}_{\mathbf{a}} \end{bmatrix} = \begin{bmatrix} \chi_{ss} & \chi_{sa} \\ \chi_{as} & \chi_{aa} \end{bmatrix} \begin{bmatrix} \hat{\mathbf{X}}_{\mathbf{s}} \\ \hat{\mathbf{X}}_{\mathbf{a}} \end{bmatrix} \tag{18}$$

where $\hat{\mathbf{X}}_{\mathbf{s}}$ and $\hat{\mathbf{X}}_{\mathbf{a}}$ are respectively the vector of structural and aerodynamic states. The matrix has been partitioned as: χ_{ss} quasi-steady aeroelastic matrix, χ_{sa} coupling term of lag terms on quasi-steady equilibrium, χ_{as} coupling term of structural states on lag terms dynamics, and χ_{aa} pure lag terms dynamics matrix.

4. LFT MODELING OF AEROELASTIC PLANTS

The aim of this section is to show the application of the LFT modeling process to the aeroelastic plant introduced in Section 3 when it is subject to uncertainties. Two analytical expressions were finally derived in Section 3 to describe the dynamic equilibrium and perform flutter analysis. Equation (18) is based in the state-space framework, while (11) is expressed in the frequency domain. These formulations are equivalent as long as all the terms involved in the plant description of (11) are rational functions of the Laplace variable s. It has been discussed that this is not the case when unsteady aerodynamics theories are employed. Of course, nominal flutter analyses of a certain plant with either equation should give reasonably close results (this will be further investigated in Subsection 5.1).

However, in robust analysis applications the different formulations of the plant have two important consequences. Firstly, the LFT model development path, interpreted here as the process followed to transform the nominal plant into the robust framework required for application of μ analysis, changes. Secondly, the effect on the results when considering aerodynamic uncertainty also changes
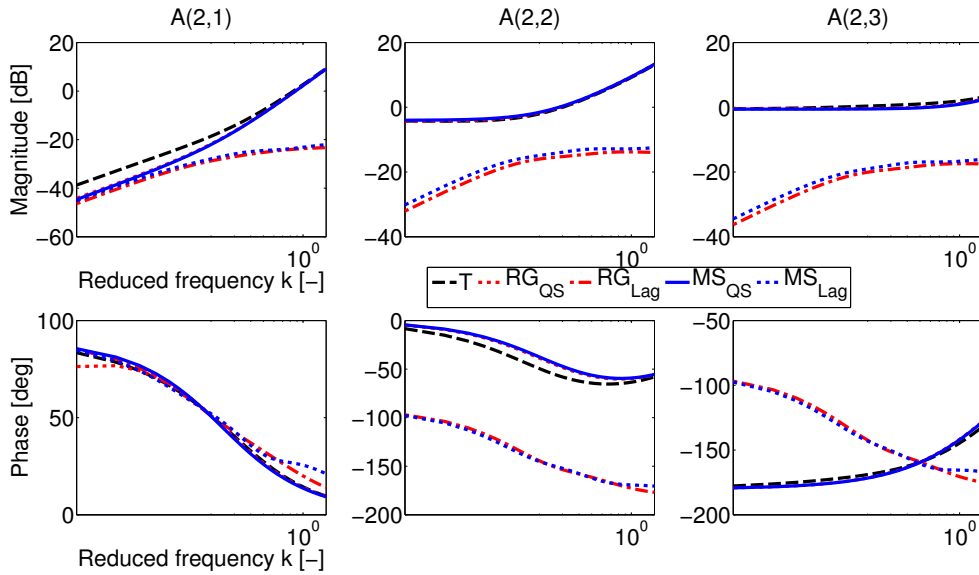
Figure 4. Bode plot of the AIC matrix for three transfer functions (Theodorsen and its approximations)

depending on the expression adopted for the AIC, whether it is the original frequency-dependent or its approximation, and in this latter case also depending on the approximation employed. The first aspect is addressed in Subsection 4.1 and the latter in Subsection 4.2.

4.1. Problem formulation

Parametric uncertainties are used to describe parameters whose values are not known with a satisfactory level of confidence. Considering a generic uncertain parameter d, with λ_d indicating the uncertainty level with respect to a nominal value d_0, a general uncertain representation is given by:

$$d = d_0 + \lambda_d \delta_d \tag{19}$$

This expression is often referred to as *additive* uncertainty. At a matrix level, the operator $\mathbf{D}$ which is affected by parametric uncertainties can be thus expressed as:

$$\begin{bmatrix} \mathbf{D} \end{bmatrix} = \begin{bmatrix} \mathbf{D_0} \end{bmatrix} + \begin{bmatrix} \mathbf{V_D} \end{bmatrix} \begin{bmatrix} \mathbf{\Delta_D} \end{bmatrix} \begin{bmatrix} \mathbf{W_D} \end{bmatrix} \tag{20}$$

where $\mathbf{D_0}$ is the nominal operator and $\mathbf{V_D}$ and $\mathbf{W_D}$ are scaling matrices which, provided the uncertainty level λ_d for each parameter, give a perturbation matrix $\mathbf{\Delta_D}$ belonging to the norm bounded subset, i.e. $\bar{\sigma}(\mathbf{\Delta_D}) \leq 1$. The proposed expression recalls the definition of an LFT in the particular case when the rational dependence on the uncertainties is set to zero (see for example Equation (3) with $\mathbf{M_{11}}$=0). Hence operators described by means of (20) are LFTs themselves. This aspect is helpful in the LFT building process since a fundamental property [28] is that interconnection of LFTs are again LFTs, thus for example it is possible to cascade, add, and invert them resulting always in an LFT.

These uncertain blocks can be obtained by, for example, writing the uncertain parameters in symbolic form and using the well consolidated LFR toolbox [11] which enables to evaluate their

expression. In order to minimise the number of repeated uncertain parameters, different realization techniques can be adopted such as *Horner factorization* or *tree decomposition* [19, 20, 29].

The next subsections show how, despite starting from this common uncertainty description, the two possible definitions of the dynamic aeroelastic equilibrium lead to distinct LFT development processes. This in turn can result in different analysis results potentially limiting their usefulness, and thus insightful and system-based modeling is necessary.

4.1.1. Frequency domain approach The process of building up the LFT associated with the nominal plant described in (11) follows the idea outlined in [6]. The general case of the dynamic equilibrium of the plant with an input force $\mathbf{U}$ is given by:

$$\left[\left[\mathbf{M_s}\right]s^2 + \left[\mathbf{C_s}\right]s + \left[\mathbf{K_s}\right] - q\left[\mathbf{A}(\bar{s})\right]\right]\mathbf{X}(s) = \mathbf{U}(s) \tag{21}$$

The idea is to recast this problem as in Figure 1(b), where $\mathbf{y} = \mathbf{X}$ and $\mathbf{u} = \mathbf{U}$. Thus a formal description of the problem is sought in the following format:

$$\begin{aligned} \mathbf{w} &= \left[\boldsymbol{\Delta}\right]\mathbf{z} \\ \mathbf{z} &= \left[\mathbf{M_{11}}\right]\mathbf{w} + \left[\mathbf{M_{12}}\right]\mathbf{U} \\ \mathbf{X} &= \left[\mathbf{M_{21}}\right]\mathbf{w} + \left[\mathbf{M_{22}}\right]\mathbf{U} \end{aligned} \tag{22}$$

The first step is to explicitly define the uncertainty dependence of the four operators in (21), i.e. $\mathbf{M_s}$, $\mathbf{C_s}$, $\mathbf{K_s}$ and $\mathbf{A}(\bar{s})$. This can be achieved by applying the additive description of (20) to the four aeroelastic operators:

$$\begin{aligned} \left[\mathbf{M_s}\right] &= \left[\mathbf{M_{s0}}\right] + \left[\mathbf{V_M}\right]\left[\boldsymbol{\Delta_M}\right]\left[\mathbf{W_M}\right] \\ \left[\mathbf{C_s}\right] &= \left[\mathbf{C_{s0}}\right] + \left[\mathbf{V_C}\right]\left[\boldsymbol{\Delta_C}\right]\left[\mathbf{W_C}\right] \\ \left[\mathbf{K_s}\right] &= \left[\mathbf{K_{s0}}\right] + \left[\mathbf{V_K}\right]\left[\boldsymbol{\Delta_K}\right]\left[\mathbf{W_K}\right] \\ \left[\mathbf{A}\right] &= \left[\mathbf{A_0}\right] + \left[\mathbf{V_A}\right]\left[\boldsymbol{\Delta_A}\right]\left[\mathbf{W_A}\right] \end{aligned} \tag{23}$$

The expressions in (23) can then be substituted back to (21) leading, at a fixed frequency ω, to:

$$\begin{aligned} \left[\mathbf{M_{22}}(\omega)\right]^{-1}\mathbf{X} &= \left[\mathbf{V}\right]\left[\boldsymbol{\Delta}\right]\left[\mathbf{W}\right]\mathbf{X} + \mathbf{U} \\ \text{with} \quad \left[\mathbf{M_{22}}(\omega)\right]^{-1} &= \left[-\omega^2\left[\mathbf{M_{s0}}\right] + i\omega\left[\mathbf{C_{s0}}\right] + \left[\mathbf{K_{s0}}\right] - q\left[\mathbf{A_0}(k)\right]\right] \end{aligned} \tag{24}$$

where $\boldsymbol{\Delta}$ is a block diagonal matrix holding the $\boldsymbol{\Delta_\bullet}$ matrices and $\mathbf{V}$, $\mathbf{W}$ are built up from $\mathbf{V_\bullet}$ and $\mathbf{W_\bullet}$ (with $\bullet = \{M, C, K, A\}$ following the operators in Equation (23)). Not that the inverse of $\mathbf{M_{22}}$ exists provided that the nominal system does not have pure imaginary eigenvalues.

Equation (24) can be finally recast in the template (22) through these final steps (we drop the frequency dependency of $\mathbf{M_{22}}$ from now on for ease of notation, unless unclear from the context):

$$\begin{aligned} \mathbf{w} &= \left[\boldsymbol{\Delta}\right]\mathbf{z}; \quad \mathbf{z} = \left[\mathbf{W}\right]\mathbf{X} \\ \left[\mathbf{M_{22}}\right]^{-1}\mathbf{X} &= \left[\mathbf{V}\right]\mathbf{w} + \mathbf{U} \\ &\begin{cases} \mathbf{X} = \left[\mathbf{M_{22}}\right]\left[\mathbf{V}\right]\mathbf{w} + \left[\mathbf{M_{22}}\right]\mathbf{U} \\ \mathbf{z} = \left[\mathbf{W}\right]\left[\mathbf{M_{22}}\right]\left[\mathbf{V}\right]\mathbf{w} + \left[\mathbf{W}\right]\left[\mathbf{M_{22}}\right]\mathbf{U} \end{cases} \end{aligned} \tag{25}$$

The last two expressions provide the sought partition of the coefficient matrix $\mathbf{M}$, at a given frequency ω:

$$\begin{bmatrix} \mathbf{M_{11}} \end{bmatrix} = \begin{bmatrix} \mathbf{W} \end{bmatrix} \begin{bmatrix} \mathbf{M_{22}} \end{bmatrix} \begin{bmatrix} \mathbf{V} \end{bmatrix}$$
$$\begin{bmatrix} \mathbf{M_{12}} \end{bmatrix} = \begin{bmatrix} \mathbf{W} \end{bmatrix} \begin{bmatrix} \mathbf{M_{22}} \end{bmatrix} \quad (26)$$
$$\begin{bmatrix} \mathbf{M_{21}} \end{bmatrix} = \begin{bmatrix} \mathbf{M_{22}} \end{bmatrix} \begin{bmatrix} \mathbf{V} \end{bmatrix}$$

It is highlighted that usually the dependence on ω is contained within $\mathbf{M_{22}}$, see Equation (24). Nonetheless, when frequency-dependent uncertainty descriptions are used for the operators in (23), then the matrices $\mathbf{V_\bullet}$ and $\mathbf{W_\bullet}$ are also dependent on ω. This is often the case for the aerodynamic operator $\mathbf{A}(\bar{s})$.

4.1.2. State-space approach This approach takes its clue from the fact that an LFT can be viewed as a realization technique [11]. Indeed the LFT formulae can be used to establish the relationship between a generic transfer matrix and its state space realization, once a proper definition for the operators $\mathbf{M}$ and $\boldsymbol{\Delta}$ is adopted:

$$\begin{cases} \dot{\mathbf{x}} = \bar{\mathbf{A}}\mathbf{x} + \bar{\mathbf{B}}\mathbf{u} \\ \mathbf{y} = \bar{\mathbf{C}}\mathbf{x} + \bar{\mathbf{D}}\mathbf{u} \end{cases}$$
$$\mathbf{G}(s) = \bar{\mathbf{D}} + \bar{\mathbf{C}}(s\mathbf{I_n} - \bar{\mathbf{A}})^{-1}\bar{\mathbf{B}} = \mathcal{F}_u(\mathbf{M}, \boldsymbol{\Delta}) \quad (27)$$
$$\mathbf{M} = \begin{bmatrix} \bar{\mathbf{A}} & \bar{\mathbf{B}} \\ \bar{\mathbf{C}} & \bar{\mathbf{D}} \end{bmatrix}; \quad \boldsymbol{\Delta} = \frac{1}{s}\mathbf{I_n}$$

This shows that a plant described through its state-space realization and affected by uncertainties can be seen as an LFT with the $\boldsymbol{\Delta}$ matrix split into two blocks: $\boldsymbol{\Delta_u}$ containing the perturbations affecting the state-space matrices, and $\frac{1}{s}\mathbf{I_n}$ as previously introduced, with $\mathbf{n}$ the number of states. The coefficient matrix $\mathbf{M}$ is partitioned correspondingly, as depicted in Figure 5.
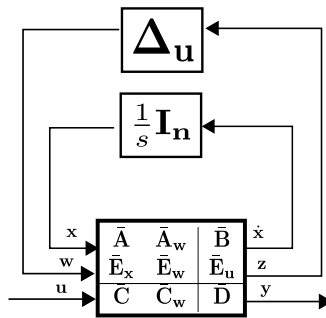
Figure 5. LFT of an uncertain state-space model

Calculating the frequency response of this LFT basically amounts to evaluating the block between $\dot{\mathbf{x}}$ and $\mathbf{x}$ at $s = \mathrm{j}\omega$. At this point, the LFT recovers to the form originally introduced in Equation (3). This means that all the four sub-matrices $\mathbf{M_{ij}}$ are defined and so the modeling process is formally completed. In particular, the transfer matrix $\mathbf{M_{11}}$ employed in (5) to assess RS of the system, is here itself an LFT formed by the terms in the upper left block of the coefficient matrix in Figure 5,

that is:

$$\mathbf{M_{11}}(s) = \bar{\mathbf{E}}_{\mathbf{w}} + \frac{1}{s}\bar{\mathbf{E}}_{\mathbf{x}}(\mathbf{I_n} - \frac{1}{s}\bar{\mathbf{A}})^{-1}\bar{\mathbf{A}}_{\mathbf{w}} = \bar{\mathbf{E}}_{\mathbf{w}} + \bar{\mathbf{E}}_{\mathbf{x}}(s\mathbf{I_n} - \bar{\mathbf{A}})^{-1}\bar{\mathbf{A}}_{\mathbf{w}}$$

$$= \mathcal{F}_u(\mathbf{P}, \boldsymbol{\Delta}); \qquad \mathbf{P} = \begin{bmatrix} \bar{\mathbf{A}} & \bar{\mathbf{A}}_{\mathbf{w}} \\ \bar{\mathbf{E}}_{\mathbf{x}} & \bar{\mathbf{E}}_{\mathbf{w}} \end{bmatrix}; \qquad \boldsymbol{\Delta} = \frac{1}{s}\mathbf{I_n} \tag{28}$$

As seen, the partitioned matrix $\mathbf{P}$ consists of the nominal state-matrix $\bar{\mathbf{A}}$ and the blocks $\bar{\mathbf{A}}_{\mathbf{w}}$, $\bar{\mathbf{E}}_{\mathbf{x}}$ and $\bar{\mathbf{E}}_{\mathbf{w}}$ arising from the plant uncertainty description.

As pointed out before, the sub-matrix $\mathbf{M_{11}}$ is pivotal in the application of μ for robust analysis. It is hence interesting at this point to draw a comparison between its expression in the two formulations presented, Equations (26) and (28). They are transfer functions depending on the inverse of the frequency response of the nominal plant, which is $(s\mathbf{I_n} - \bar{\mathbf{A}})$ for the latter and $\mathbf{M_{22}}^{-1}$ for the former one. These terms are then pre-post multiplied by non-square *scaling* matrices describing the effect of the perturbations on the system.

On the other hand, the *scaling* matrices involved in the two definitions ($\mathbf{V}$ and $\mathbf{W}$ in Equation (26) and $\bar{\mathbf{A}}_{\mathbf{w}}$, $\bar{\mathbf{E}}_{\mathbf{x}}$ and $\bar{\mathbf{E}}_{\mathbf{w}}$ in Equation (28)) are inherently different. They are directly derived from the uncertainty definition, which in one case applies to the aeroelastic operators gathered in (15), whereas in the other are those from (21). These reflections are preparatory of the result given at the end of this section which unifies these LFT models.

This subsection has shown the main steps to recast the aeroelastic plant into the LFT framework when the starting point is formulated in the frequency or time domain. As stressed in Sec. 3, Equation (11) is prototypical of current industrial state-of-practice models used for linear flutter stability, where the structural matrices are generally provided by Finite Element Method (FEM) codes and the AIC matrix by means of DLM solvers. This motivates the adoption of the typical section to investigate the robust modeling and analysis tasks for this aeroelastic problem.

However, when employing this paradigm for real (e.g. full aircraft) applications, it is expected that practical issues would arise. Among these, the increase in the size of the problem can be identified as one of the most compelling. A solution, borrowed from the aeroelastic community, consists in applying a modal decomposition to the original large-scale equations and considering only the reduced set for modeling and analysis. Typically for aircraft flutter predictions only the first 5-6 modes are retained as significant for the instability mechanism [24]. A more sophisticated two-step procedure, consisting in firstly reducing the reference models with advanced methods and then building the LFT model by means of polynomial interpolation, was discussed in [15] and is particularly suited for the generation of models used for control system design and analysis.

Adding to this, an issue originated from the order reduction is the difficult reconciliation between the uncertain parameters (defined in the reduced model) and the physical sources of uncertainties (well distinguishable in the original model). This can be tackled with modern polynomial interpolation techniques [30], which enables the influence of the physical parameters in the reduced models to be efficiently captured, or by applying the LFT modeling to the original operators and then reduce the LFT size by means of the modal decomposition. The latter methodology enables the uncertain parameter to be associated with the physical one, at the cost of neglecting its effect on the modes (which are kept at their nominal values in the decomposition). The effect of this assumption in

real applications has been evaluated in [31], where possible strategies to limit the impact of this assumption are also discussed.

4.2. Uncertainties in the aerodynamic operator

The aerodynamic operator, giving a relation between the elastic degrees of freedom and the corresponding loads over the wing section, is one of the most relevant features of aeroelastic modeling.

The different expressions of the unsteady AIC matrices were discussed in Section 3. The one introduced in (9), hereafter named $\mathbf{A}_T$, is the true aerodynamic operator given by Theodorsen theory, or alternatively provided by a frequency domain based panel method solver (e.g. DLM). When the problem needs to be recast in state-space, approximate operators are used: in this work Roger approximation $\mathbf{A}_{Rg}$ and Minimum State approximations $\mathbf{A}_{MS}$ are employed. In particular, (12) shows that both algorithms involve a general two-part approximation model based on *quasi-steady* and *lag* physical contributions. The adoption of an unsteady formulation implies a choice of pursuing the LFT modeling by means of either the approach in Subsection 4.1.1 or by the one in Subsection 4.1.2. This will be shown to be significant since the aerodynamics operator and its uncertainties are handled differently.

In the latter case, the LFT development leads to the framework of Figure 5 where uncertainties are specified in the state matrices. If for example the state-matrix for the Roger approximation detailed in (15) is recalled (similar observations can be inferred for the Minimum State case), it is clear that uncertainties can only be expressed in the single terms defining the approximation, such as for example the real coefficient matrices $\mathbf{A_i}$ or the aerodynamics lags γ_j.

Conversely, when the LFT modeling is performed starting from (11), the *original* complex valued AIC matrix $\mathbf{A}_T$ explicitly appears in the plant and the uncertainties can be directly specified in the generic term $A_{T_{ij}}$ representing the transfer function from the jth degree of freedom in $\mathbf{X}^E$ to the ith aerodynamic load component in $\mathbf{L_a}^E$.

As a preliminary to the discussion on the role of uncertainties in the aerodynamics operators, the rationale underpinning their selection is discussed here.

The results relative to nominal analysis, shown in Sec. 5.1, will highlight that these different approaches (state-space/frequency domain and then rational approximations/Theodorsen) lead to identical results in terms of *nominal* flutter speed. This is to remark that the uncertainty description of the approximate operators $\mathbf{A}_{Rg}$ and $\mathbf{A}_{MS}$ is not formulated to balance out deficiencies with respect to the irrational true operator. The chief goal of the uncertain aerodynamics description considered here, whether it is applied to the operator $\mathbf{A}_T$ (analogously to the DLM one, which, as stated, relies on similar hypotheses) or its rational approximations, is to compensate for limits of validity of the physical assumptions underlying the aerodynamic model (e.g. potential and incompressible flow).

The proposed strategy assumes that reference data, describing the aerodynamic behavior of the body with improved accuracy, are available. They can originate from experimental data or high fidelity Computational Fluid Dynamics (CFD) simulations, and in both cases are typically able to provide a frequency domain description of the relation displacement-load as in (9). In case of nonlinear simulations, these can be obtained by linearizing the response about the studied operating point.

Once these data are available, and a set of uncertain parameters in the model are selected (possible

choices will be described later in this section), the μ-based model validation technique proposed in [32] can provide a rationale to allocate the amount of uncertainty in the system. In particular, a μ test applied to the LFT model of the uncertain plant is able to conclude whether it generates the reference data (i.e. a type of model validation test). In other words, the uncertainty description (in terms of uncertain terms and corresponding uncertainty levels λ_i) can be tailored such that the results observed experimentally or numerically lie within the uncertainty set defined by the LFT. This approach would therefore enable simplifying and low order mathematical models to be adopted, achieving at the same time a broader validity of the predicted results. An alternative to the method in [32] is proposed at the end of Subsection 4.2.1, where the worst-case gain of the aerodynamic operator is employed as metric to correlate two families of aerodynamic data.

4.2.1. Reconciliation of the different LFT descriptions Next we focus on the *aerodynamic* LFT $\mathcal{F}_u(\hat{\mathbf{A}}, \boldsymbol{\Delta})$ (where $\hat{\mathbf{A}}$ refers to $\hat{\mathbf{A}}_T$, $\hat{\mathbf{A}}_{Rg}$ or $\hat{\mathbf{A}}_{MS}$ depending on which LFT is employed), which is a description of the uncertain aerodynamic operator. A first analysis (Case 1) is performed on the LFTs of Figure 6. The left-most LFT, $\mathcal{F}_u(\hat{\mathbf{A}}_T, \boldsymbol{\Delta_T})$, describes the AIC matrix given by the Theodorsen theory when uncertainties in the three transfer functions $A_{T_{12}}$, $A_{T_{21}}$ and $A_{T_{22}}$ are considered (respectively, the ones between pitch α and lift L, plunge h and pitching moment M_α, and pitch α and pitching moment M_α). The uncertainty description is such that *at each frequency* they range in the disc of the complex plane centered in the nominal value and having a radius equal to 10% of its magnitude. Note that this kind of weight is a non rational function of the frequency since it *follows* the nominal value of the parameter in its variation within the frequency range considered, i.e. the matrices $\mathbf{V_A}$ and $\mathbf{W_A}$ have an arbitrary, that is not necessarily rational, dependence on frequency.
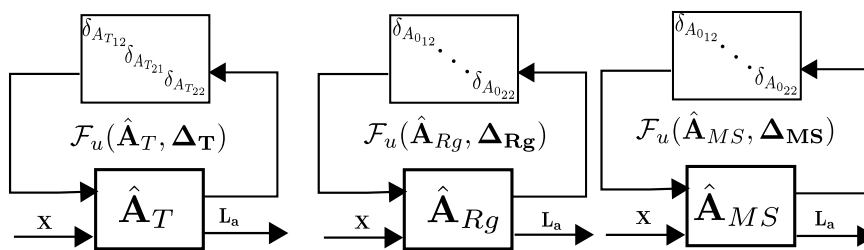

Figure 6. Example of LFTs with aerodynamic uncertainties

The LFTs $\mathcal{F}_u(\hat{\mathbf{A}}_{Rg}, \boldsymbol{\Delta_{Rg}})$ and $\mathcal{F}_u(\hat{\mathbf{A}}_{MS}, \boldsymbol{\Delta_{MS}})$ describe respectively the transfer matrices $\mathbf{A}_{Rg}$ and $\mathbf{A}_{MS}$ when uncertainties in the *quasi-steady* part of the approximation $\boldsymbol{\Gamma}_{QS}$ are considered. Recalling its definition from (13), this means that $\mathbf{A_2}$, $\mathbf{A_1}$ and $\mathbf{A_0}$ are affected. The same three transfer functions as above are considered (note however that $A_{0_{21}}$ is always null in this formulation). The unsteady component of the approximation is for now defined without uncertainty. For the algorithmic implementation of Roger method, four aerodynamic roots equally spaced between -0.1 and -0.7 were selected, while for the Minimum State method, six aerodynamic roots equally spaced between -0.1 and -0.7 were retained. The approximation is performed in the range of reduced frequency k $\in [0.01; 1.5]$.

The resulting upper LFTs are defined by the uncertain blocks below:

$$\Delta_{\mathbf{T}}^{3,C} = \mathrm{diag}(\delta_{A_{T_{12}}}, \delta_{A_{T_{21}}}, \delta_{A_{T_{22}}})$$
$$\Delta_{\mathbf{Rg}}^{8,R} = \Delta_{\mathbf{MS}}^{8,R} = \mathrm{diag}(\delta_{A_{0_{12}}}, \delta_{A_{0_{21}}}, \delta_{A_{0_{22}}}, \delta_{A_{1_{12}}}, \delta_{A_{1_{21}}}, \delta_{A_{1_{22}}}, \delta_{A_{2_{12}}}, \delta_{A_{2_{21}}}, \delta_{A_{2_{22}}})$$
(29)

where the size of the uncertainties (total Δ dimension) and their nature (real R or complex C) is recalled in the superscripts. Each parameter is assigned the *same* uncertainty level of 10%. A comparison in terms of the uncertain frequency response of the transfer function $\frac{M_\alpha}{\alpha}$ as a function of k is shown in Figure 7 for the three (T, Rg and MS) cases.
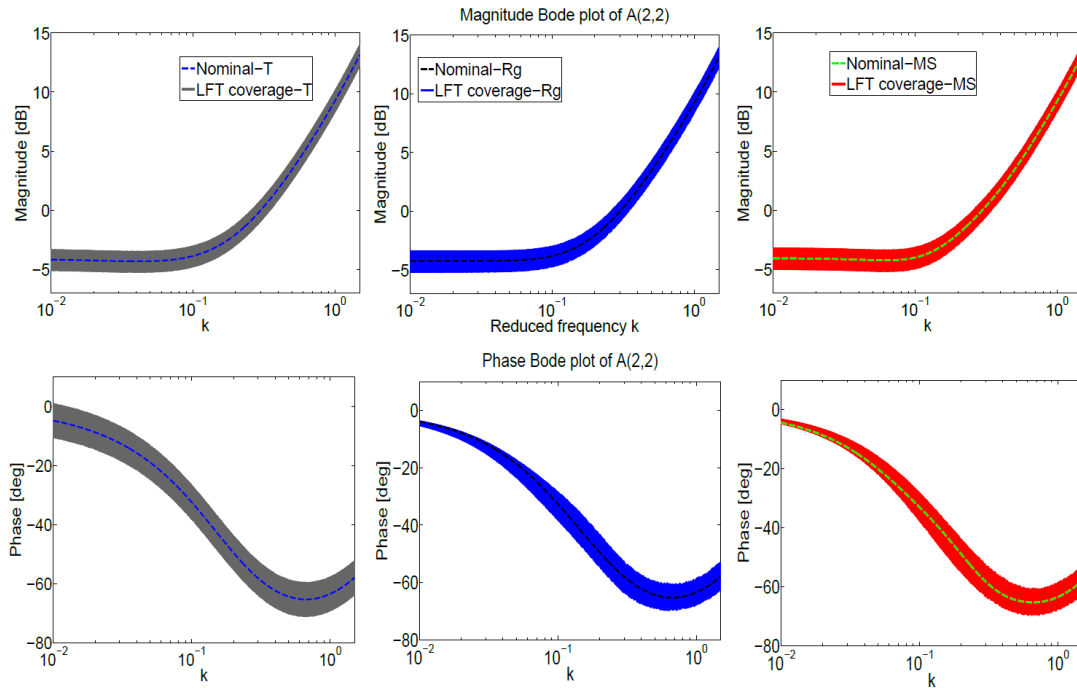
Figure 7. Frequency response of the transfer function $\frac{M_\alpha}{\alpha}$ for the three aerodynamic LFTs, Case 1

The LFT coverage is obtained evaluating $\mathcal{F}_u(\hat{\mathbf{A}}, \Delta)$ at random values of the uncertainty block. The coloured area, here labeled as LFT *coverage*, can be interpreted as the family of transfer functions originated by the provided uncertainty description. In the case of the approximated operators $\mathcal{F}_u(\hat{\mathbf{A}}_{Rg}, \Delta_{\mathbf{Rg}})$ and $\mathcal{F}_u(\hat{\mathbf{A}}_{MS}, \Delta_{\mathbf{MS}})$, the families are almost overlapping, while for $\mathcal{F}_u(\hat{\mathbf{A}}_T, \Delta_{\mathbf{T}})$ it appears to cover a larger area in respect of the phase plot.

A comparison between these two families of plants, on one side the two LFTs originating from the rational approximations and on the other side the LFT associated with the Theodorsen operator, is not straightforward. Although the same transfer functions are affected by perturbations in their nominal values, the uncertainty description is different both in terms of captured features (in the first only the quasi-steady part is involved, while in the second the whole transfer function) and in terms of number of uncertainties (see Equation (29)). Thus, no clear correspondence from one description to another exists. The technique employed to obtain Figure 7 however gives physical insight into the LFT. For instance, it suggests how the choice of taking into account only the quasi-steady part

in $\mathbf{\Delta_{MS}}$ and $\mathbf{\Delta_{Rg}}$ determines a narrower coverage of the phase diagram relative to $\mathbf{\Delta_T}$, which does not have such distinction (this makes sense as we are restricting the effects of the former).

Then, a second case is considered (Case 2) which captures uncertainty only in the unsteady part of the approximated operators, assuming a variation in the value of the lag roots. The uncertainty blocks are defined below, using again the *same* uncertainty level of 10% for each parameter:

$$
\begin{aligned}
\mathbf{\Delta_{Rg-L}}^{4,R} &= \mathrm{diag}(\delta_{\gamma_1}, \delta_{\gamma_2}, \delta_{\gamma_3}, \delta_{\gamma_4}) \\
\mathbf{\Delta_{MS-L}}^{6,R} &= \mathrm{diag}(\delta_{\gamma_1}, \delta_{\gamma_2}, \delta_{\gamma_3}, \delta_{\gamma_4}, \delta_{\gamma_5}, \delta_{\gamma_6})
\end{aligned}
\tag{30}
$$

In Subsection 3.1 it was discussed that the lag roots are the cross-over frequencies of the high-pass filters approximating the unsteadiness of the flow, which produce a magnitude decrease and a phase shift compared to that for the quasi-steady case. Figure 7 showed that an uncertainty description affecting only the quasi-steady part of the approximation does not fully capture the phase frequency response variability seen in the perturbed plants from the family $\mathcal{F}_u(\hat{\mathbf{A}}_T, \mathbf{\Delta_T})$. As is well known, the phase shift generated by a high-pass filter at a fixed frequency is dependent only on its cross-over frequency and is unrelated to the gain a. In fact it is true that:

$$
\begin{aligned}
H(\bar{s}) &= \frac{a\bar{s}}{\bar{s} + \gamma}; \qquad \bar{s} = ik \\
H(ik) &= \frac{a\,ik}{ik + \gamma} = \frac{ak^2 + iak\gamma}{k^2 + \gamma^2}; \qquad \arg(H) = \tan^{-1}(\frac{\gamma}{k})
\end{aligned}
\tag{31}
$$

This is the reason why the uncertainty blocks in (30) are defined so as to capture variations in the terms responsible for the phase shift. From a physical point of view, this indeed allows inaccuracies in the estimation of the unsteady part of the loads, of which the phase shift is a crucial feature, to be modelled. Equation (31) provides also a quantitative indication of the effect on the frequency response of uncertain lag roots, and thus it can be used to calibrate the amount of uncertainty in them, based on experimental or numerical data describing the expected aerodynamic behavior in terms of load generation. Note for example that the lag root effect in phase shifting highly depends on the reduced frequency k considered, and thus a weight function of the frequency is envisaged to properly model this uncertainty.

Again, a comparison is performed in Figure 8, but now the frequency responses (only magnitude for brevity) of all the transfer functions involved in the plunge and pitch equilibria are shown.
The first conclusion inferred by these plots is that the two LFTs with the same uncertainty level in the lag roots lead to considerably different plants. This was somehow expected since there is a substantial difference in the definition of $\mathbf{\Gamma}_{lag-Rg}$ and $\mathbf{\Gamma}_{lag-MS}$, as stressed in the comments of (14) and (17) where they are respectively defined, and thus uncertainties in those terms have different effects on the plant.

A second important observation is that all the frequency responses (i.e. aerodynamic transfer functions) are affected by these uncertainty descriptions. This is the consequence of the approximation formula, where each high-pass filter influences all the terms in the transfer matrix. This is different from what happens for the aerodynamic LFT based on the Theodorsen operator $\mathcal{F}_u(\hat{\mathbf{A}}_T, \mathbf{\Delta_T})$, where the uncertainty is specified directly in each term of the transfer function and thus only the corresponding frequency response is affected.
This is an important feature to highlight about the LFT modeling process, since it shows that defining

uncertainty for the lag terms of the approximations (in order to capture uncertainty in the unsteady part of the aerodynamic model), automatically implies uncertainty in all the transfer functions. Thus, a comparison with the plant families originating from the definition of $\mathbf{\Delta_T}$ is not possible in this case.

This section is concluded with an approach proposed to correlate the maps $\mathcal{F}_u(\hat{\mathbf{A}}_{Rg}, \mathbf{\Delta_{Rg-L}})$ and $\mathcal{F}_u(\hat{\mathbf{A}}_{MS}, \mathbf{\Delta_{MS-L}})$ (case of uncertainties in the lags). The mismatch exhibited in Figure 8 has to be ascribed to a different *amount* of uncertainty within the two operators, and not to a different *effect* of the uncertainties in the plant, as is the case previously discussed for $\mathcal{F}_u(\hat{\mathbf{A}}_T, \mathbf{\Delta_T})$.

A straightforward strategy to correlate these families could be to iterate the plots in Figure 8 until a satisfactory overlapping is obtained. However, this procedure is time consuming and ambiguous since at least two objectives, magnitude and phase, for each transfer function must be considered.
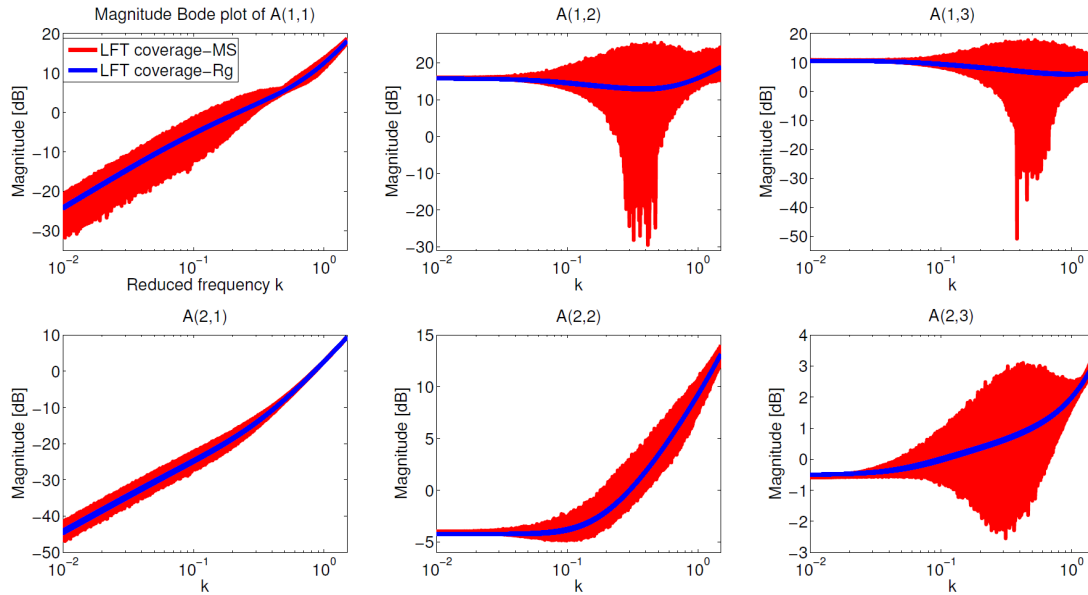
Figure 8. Six frequency responses (magnitude) for the LFTs $\hat{\mathbf{A}}_{Rg}$ and $\hat{\mathbf{A}}_{MS}$, Case 2 (uncertainties in the lag roots with same uncertainty level)

The procedure proposed here focuses on the norm-magnitude of the two LFTs. In particular, the worst-case H_∞ norm of the aerodynamic operator could be used to relate the amount of uncertainty in the two different sets. The command *wcgain* of the Robust Control Toolbox (RCT) in MATLAB [33] is employed here for this purpose. The idea is to define the *aerodynamic worst-case gain* WC_G^A as a function of the maximum allowed norm $\bar{\alpha}$ of the uncertainty matrix:

$$WC_G^A(\mathcal{F}_u(\hat{\mathbf{A}}, \mathbf{\Delta}), \bar{\alpha}) = \max_{\|\mathbf{\Delta}\|_\infty \leq \bar{\alpha}} \|\mathcal{F}_u(\hat{\mathbf{A}}, \mathbf{\Delta})\|_\infty \qquad (32)$$

Once the size $\bar{\alpha}$ is fixed, WC_G^A could represent a term of comparison among different uncertainty descriptions. For example, it is here considered a given *reference* LFT $\mathcal{F}_u(\hat{\mathbf{A}}^\mathbf{r}, \mathbf{\Delta}^\mathbf{r})$ and a *tested* LFT $\mathcal{F}_u(\hat{\mathbf{A}}^\mathbf{t}, \mathbf{\Delta}^\mathbf{t})$ which has to be defined such that $\mathbf{\Delta}^\mathbf{t}$ maps $\hat{\mathbf{A}}^\mathbf{t}$ in a similar family of plants than $\mathcal{F}_u(\hat{\mathbf{A}}^\mathbf{r}, \mathbf{\Delta}^\mathbf{r})$. An algorithm is proposed next to address this task by determining the amount of uncertainty held in $\mathcal{F}_u(\hat{\mathbf{A}}^\mathbf{t}, \mathbf{\Delta}^\mathbf{t})$, expressed by means of the uncertainty levels λ_i of the n_p parameters gathered in $\mathbf{\Delta}^\mathbf{t}$.

Algorithm 1

<u>Output</u>: The uncertainty levels vector $\mathbf{\Lambda} = [\lambda_1 ... \lambda_i ... \lambda_{n_p}]^T$ which ensures a consistent mapping between the two LFTs

<u>Inputs</u>: reduced frequency k; the reference $\mathcal{F}_u(\hat{\mathbf{A}}^{\mathbf{r}}, \mathbf{\Delta}^{\mathbf{r}})$ (normalized such that $\bar{\sigma}(\mathbf{\Delta}^{\mathbf{r}}) \leq 1$) and the tested $\mathcal{F}_u(\hat{\mathbf{A}}^{\mathbf{t}}, \mathbf{\Delta}^{\mathbf{t}})$ (with uncertainty ranges given in the vector $\mathbf{\Lambda}$) LFTs; a first guess $\mathbf{\Lambda}^0$; and tolerance parameter ϵ on the result

1. Find $WC_G^{A,r}$ using Equation (32), $\mathcal{F}_u(\hat{\mathbf{A}}^{\mathbf{r}}, \mathbf{\Delta}^{\mathbf{r}})$, and $\bar{\alpha}^r$=1
2. Using the uncertainty vector $\mathbf{\Lambda}$ (for the first iteration use the initial guess $\mathbf{\Lambda}^0$), normalize $\mathcal{F}_u(\hat{\mathbf{A}}^{\mathbf{t}}, \mathbf{\Delta}^{\mathbf{t}})$ such that $\bar{\sigma}(\mathbf{\Delta}^{\mathbf{t}}) \leq 1$
3. Find $WC_G^{A,t}$ using Equation (32), $\mathcal{F}_u(\hat{\mathbf{A}}^{\mathbf{t}}, \mathbf{\Delta}^{\mathbf{t}})$, and $\bar{\alpha}^t = \bar{\alpha}^r$
4. If $\frac{WC_G^{A,r} - WC_G^{A,t}}{WC_G^{A,r}} = \delta_{WC} > \epsilon$, update the uncertainty vector $\mathbf{\Lambda} = (1 + \delta_{WC})\mathbf{\Lambda}$ and repeat the iteration from Step 2 until $\delta_{WC} \leq \epsilon$.

Remark 1

The proposed update rule does simply update the vector of uncertainty levels by uniform scaling. Alternatively, based on the understanding of the role of the uncertain parameters, one can define a vector of weights $\mathbf{k_w}$ and take $\mathbf{\Lambda} = (1 + \delta_{WC}\mathbf{k_w}) * \mathbf{\Lambda}$. As initial guess $\mathbf{\Lambda}^0$ it can be taken the corresponding vector used in $\mathcal{F}_u(\hat{\mathbf{A}}^{\mathbf{r}}, \mathbf{\Delta}^{\mathbf{r}})$.

Remark 2

The algorithm can be restarted from Step 1 employing different values for $\bar{\alpha}^r = \bar{\alpha}^t$. Based on the authors' experience, this has barely any influence on the determination of $\mathbf{\Lambda}$, i.e. the algorithm will provide different values of WC_G^A but convergence is attained for approximately the same uncertainty levels.

Remark 3

It is implicit in the LFT definition that this algorithm is evaluated at a fixed reduced frequency, i.e. $\mathbf{\Lambda}(k)$. If the dependence on k is not negligible, i.e. $\mathbf{\Lambda}(k) \ncong \mathbf{\Lambda}$, this can be accounted for with frequency-varying weights (recall $\mathbf{V_A}$ and $\mathbf{W_A}$ from Equation 23).

This approach is proposed here to address the issue of calibrating the amount of uncertainty in the lag terms to consistently define two LFTs derived by different rational approximations. However, it is noted that it can be employed in a more general manner to inform the selection of the number/type of uncertain parameters and their range in order to *cover* (in an LFT sense) a family of frequency responses (reference data) obtained through experimental campaign or numerical analysis. In this more general case Step 1 is not needed and $WC_G^{A,r}$ is provided by the maximum singular value of the reference frequency responses.

Figure 9 shows the results of the application of this criterion to the families initially depicted in Figure 8 when $\mathcal{F}_u(\hat{\mathbf{A}}^{\mathbf{r}}, \mathbf{\Delta}^{\mathbf{r}}) = \mathcal{F}_u(\hat{\mathbf{A}}_{Rg}, \mathbf{\Delta}_{\mathbf{Rg-L}})$ (with 10% of uncertainty in each lag) and $\mathcal{F}_u(\hat{\mathbf{A}}^{\mathbf{t}}, \mathbf{\Delta}^{\mathbf{t}}) = \mathcal{F}_u(\hat{\mathbf{A}}_{MS}, \mathbf{\Delta}_{\mathbf{MS-L}})$. A satisfactory overlapping between the two families of transfer functions is achieved.

4.2.2. A unified approach As emphasized in Subsection 4.2.1, there are intrinsic difficulties in reconciling the aerodynamic uncertainty description made within the frequency domain framework with the one derived from a state-space formulation. In fact, in principle the latter only allows
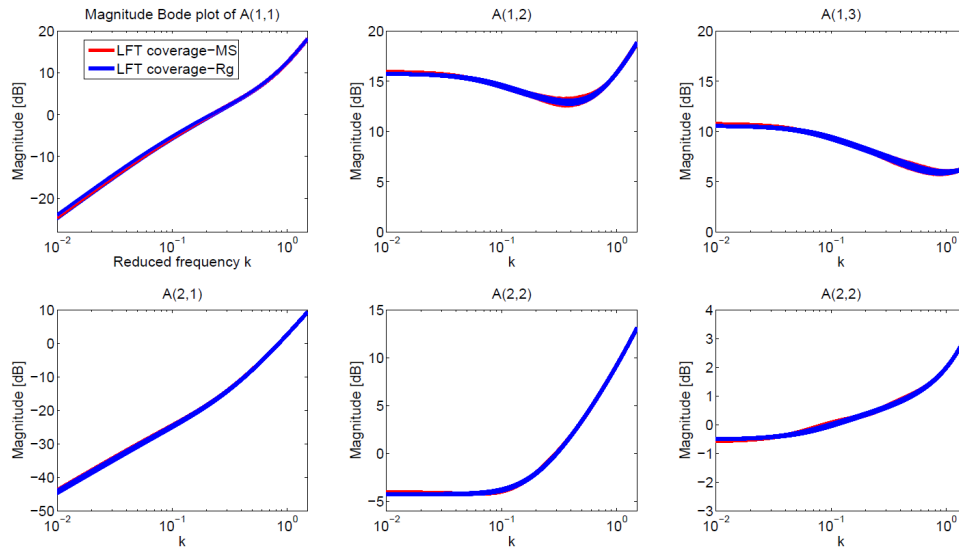
Figure 9. Six frequency responses (magnitude) for the LFTs $\hat{\mathbf{A}}_{Rg}$ and $\hat{\mathbf{A}}_{MS}$, Case 2 (uncertainties in the lag roots with weighted uncertainty level for $\mathbf{\Delta_{MS-L}}$)

uncertainties to be applied to the building blocks of the approximated operators. This means that the uncertainties are either introduced only in the quasi-steady part (not capturing the phase frequency response variability) or in the lag terms of the unsteady part (but this implies a perturbation in all the terms of the AIC matrix, and not only to a specific transfer function).

On the other hand, there are clear advantages to adopting the uncertainty description allowed by the frequency domain framework. First, this could help to take into account physical considerations in the uncertainty definition. For instance, if a lack of accuracy, based on the evidence of experimental results, is detected in the transfer function between the pitch deformation and the lift force (i.e. the $A_{T_{12}}$ term), one could model it directly. Also, matrix coefficients are complex and so are the associated uncertainties, with notable improvement on the accuracy and computation time of the μ results. Another aspect is that in this case the weighting matrices defining the range of variation of the uncertainties can have any type of dependence on the frequency (recall $\mathbf{V_\bullet}$ and $\mathbf{W_\bullet}$ in Equation 4.2), while in the former approach the rational dependence constraint holds. For current industrial state-of-practice (which relies on frequency domain aerodynamic operators for flutter analyses), this also ensures that both nominal and robust stability refer to the same aerodynamics operator (i.e. no approximations are inserted during the process). All these different aspects are highlighted in the modeling and analysis examples throughout the paper.

It is worth remarking however that these observations are only pertinent if robust flutter stability analysis is of interest. This may change when other tasks are involved, for example robust control design for flutter suppression and/or on-line robust predictions during flight tests. Indeed, these tasks have only been demonstrated using the state-space approach [8, 34], since well-consolidated algorithms dictated which framework had to be employed. The appeal of a unified framework which keeps the advantages of both the approaches is hence natural.

At this point, it is helpful to recall the definitions of the matrix $\mathbf{M_{11}}$ employed by the μ algorithm for RS analysis in the two cases. The expressions, given in (26) and (28), were derived and commented on in Subsection 4.1.1 and 4.1.2 respectively. In this regard the only restriction in

providing an aerodynamic uncertainty description for the state-space formulation akin to what is done in the frequency domain lies in the *scaling* matrices. In fact, they are not a function of the frequency in (28), whereas in (26) they are allowed to vary and are built at each frequency point. Due to the μ bounds algorithmic implementation, the calculation implies a gridding of the analysed frequency range. As a result, it is proposed to express $\mathbf{M_{11}}$ for the plant described in state-space as shown below:

$$\mathbf{M_{11}}(s, \bar{s}) = \bar{\mathbf{E}}_\mathbf{w}(\bar{s}) + \bar{\mathbf{E}}_\mathbf{x}(\bar{s})\big(s\mathbf{I_n} - \bar{\mathbf{A}}\big)^{-1}\bar{\mathbf{A}}_\mathbf{w}(\bar{s}) \tag{33}$$

In the above equation, the (non-rational) dependence on the dimensionless Laplace variable $\bar{s}$ is emphasized. Note however, that the nominal plant is still represented by $\bar{\mathbf{A}}$, i.e. the expression in (18) is still used to model it.

The last remaining task is to obtain the scaling matrices in (33). Consider the prototype aeroelastic system represented in (15) when the Roger approximation is adopted. The uncertainty description associated with the structural parameters is unaffected and follows the steps already outlined. For the aerodynamic uncertainties, it is observed that only the aeroelastic stiffness matrix $\mathbf{K}$, defined in (16), is involved. Recall indeed (Equation 9) that the unsteady aerodynamic solver provides a relation between *displacements* and loads. This matrix can thus be written as:

$$\big[\mathbf{K}\big] = \big[\mathbf{K}_s\big] - \frac{1}{2}\rho_\infty V^2 \big[\mathbf{A}_0\big] - \big[\mathbf{V_A}(\bar{s})\big]\big[\mathbf{\Delta_A}\big]\big[\mathbf{W_A}(\bar{s})\big] \tag{34}$$

in analogy with the description proposed for the frequency domain formulation in (23). The last block is built starting from the uncertainty matrix $\mathbf{A_T^\delta}$:

$$\begin{aligned}
\big[\mathbf{A_T^\delta}(\bar{s})\big] &= \big[\mathbf{V_A}(\bar{s})\big]\big[\mathbf{\Delta_A}\big]\big[\mathbf{W_A}(\bar{s})\big] \\
A_{T_{ij}}^\delta(\bar{s}) &= \|A_{T_{ij}}(\bar{s})\|\lambda_{A_{T_{ij}}}(\bar{s})\delta_{A_{T_{ij}}}
\end{aligned} \tag{35}$$

where $\delta_{A_{T_{ij}}}$ is a norm-bounded complex scalar $\big(\|\delta_{A_{T_{ij}}}\| \leq 1\big)$, $\|A_{T_{ij}}(\bar{s})\|$ is the radius of the uncertainty disc in the complex plane associated with the ij^{th} term of the *original* complex valued AIC matrix and $\lambda_{A_{T_{ij}}}(\bar{s})$ is the relative level of uncertainty (a generic function of the frequency). This description is equivalent to what is done in the frequency domain, except that the nominal value is null as this is already included in the nominal plant $\bar{\mathbf{A}}$ (i.e. the nominal aerodynamics part is provided by the rational approximation). At each frequency of the grid the expression of the state-matrix with uncertainties is defined (making use of Equations 34-35 for the aerodynamic part) and the calculation for $\mathbf{M_{11}}$ (33) can be performed. Sweeping the analysed frequency range enables the frd object to be created as input for the μ calculation.

Note that the proposed strategy, which will be validated with the analyses shown in Subsection 5.4, can also be interpreted as a particular application of an *unmodelled dynamics* uncertainty definition [33].

5. ROBUST FLUTTER ANALYSIS

Nominal flutter analysis studies the conditions at which the dynamic aeroelastic system, at a fixed, known condition, loses its stability. This is a parameter-dependent problem, since as a parameter of the model is varied the system's behavior changes. Generally, this is accomplished considering the

air stream *speed* V as the critical parameter, and the result is the definition of a speed V_f, called flutter speed, such that for all the speeds below it the system is stable.

Robust flutter analysis deals with flutter instability predictions when the aeroelastic model is subject to uncertainties. The model can be uncertain for different reasons, e.g. low confidence in the values of parameters and coefficients of the matrices or dynamics which are neglected in the nominal model. We will consider the uncertainty description framework outlined in Section 4.

Once the uncertainties affecting the model are defined, robust flutter analysis assesses at a fixed subcritical speed (i.e. lower than the nominal flutter speed) if the system is stable in the face of all the possible perturbations. In this section this task is addressed by means of the structured singular value using the algorithms as currently implemented in the RCT in MATLAB R2015b.

5.1. Nominal flutter

In principle, it is possible to solve the flutter problem studying either (11) or (18). In the latter case, the spectrum of the state-matrix is evaluated as the speed is increased from a very low value where the system is known to be stable. A crossing of the imaginary axis by one of the eigenvalues detects the onset of flutter instability.

The former approach is the most reliable and currently adopted since this is the framework where the aerodynamic loads are more accurately expressed for flutter analyses purposes. In this case the objective is to find the flutter determinant roots s in Equation (11) such that nonzero solutions for the degrees of freedom vector $\mathbf{X}$ exist. The complexity arises since the AIC matrix does not have a polynomial dependence on s and thus iterative solutions have to be sought. In literature, this has been a widely discussed topic, see for example [1], with the three major methods known as: k method, p-k method and g method.

In this work two approaches are implemented: the state-space eigenvalue analysis (with two possible options in the aerodynamic approximation) and the p-k method [35] for the frequency domain analysis.

Using the model previously presented, and the data from Appendix A, Fig. 10 shows the poles location of the three model states as the speed increases. The analysis shown in Figure 10 starts at a low speed (V=60 $\frac{m}{s}$ identified in the figure with a square marker) and consists of tracking the eigenvalues for the three elastic modes (plunge, pitch and flap). As reported in [26], the system exhibits a violent plunge-pitch flutter, featured by a merging of the frequencies just before the instability occurs (the location of the poles at the slightly subcritical speed V= 290 $\frac{m}{s}$ is highlighted with an asterisk). This flutter, due to the close interaction of the first two modes, is often referred to as *binary flutter* and ω_f indicates the frequency at flutter speed for the unstable mode. Flutter speed matches with that in [26], which is at about 303 $\frac{m}{s}$. If the plots in Figure 3 are recalled, it can be noted that the response in Figure 3(a), corresponding to a subcritical speed (V=295 $\frac{m}{s}$), shows that a disturbance (due here to a non-zero initial condition) is damped out. On the contrary, the response in Figure 3(b), obtained at a speed greater than the flutter speed (V=307 $\frac{m}{s}$), demonstrates that the system is unstable featuring increasing amplitude of oscillation at each cycle.

Table I summarizes the results obtained with the different approaches. No substantial mismatches are found in the nominal flutter speeds and frequencies predicted.

In the next sections, μ analysis is applied to the system in order to evaluate its robustness. A subcritical speed (i.e. such that the system is nominally stable) of 270 $\frac{m}{s}$ is selected.
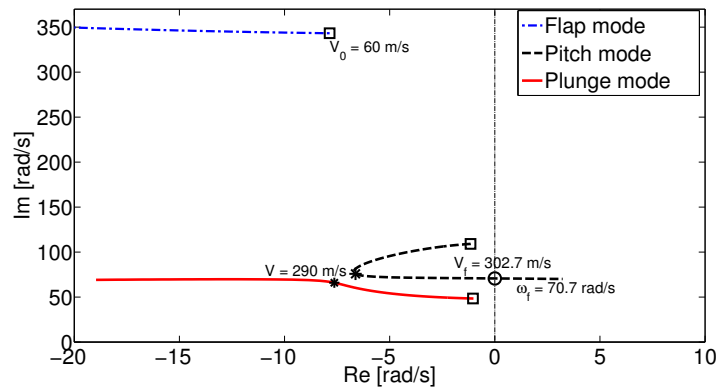
Figure 10. Poles location of the control surface, pitch and plunge modes as speed increases

Table I. Comparison of nominal flutter analyses among the different approaches

Model	Flutter velocity	Flutter frequency
State Space - Roger	302.7 $\frac{m}{s}$	11.25 Hz
State Space - Minimum State	302.5 $\frac{m}{s}$	11.2 Hz
Frequency domain p-k	301.8 $\frac{m}{s}$	11.2 Hz
Baseline [26]	303.3 $\frac{m}{s}$	11.15 Hz

5.2. Structural uncertainty analysis

The first analyses are performed taking into account uncertainties in the coefficients of the structural mass $\mathbf{M_s}$ and stiffness $\mathbf{K_s}$ matrices. In particular the uncertainty definition consists of a range of variation of 10% from the nominal value for M_{s11}, M_{s22}, K_{s22} and of 5% for M_{s12} and K_{s11}. After applying the two LFT modeling approaches discussed, using for each of the aforementioned parameters the multiplicative uncertain model of (19), the resulting LFT with uncertainty block $\mathbf{\Delta_s}^{6,R}$ given below is obtained (recall that the subscript indicates structural uncertainties, while the superscript the total uncertainty dimension and its nature):

$$\mathbf{\Delta_s}^{6,R} = \text{diag}(\delta_{Ms11}, \delta_{Ms12}I_2, \delta_{Ms22}, \delta_{Ks11}, \delta_{Ks22}) \tag{36}$$

Since only structural parameters affect the uncertainty blocks, no mismatch in principle is expected when adopting either the state-space (SS) or the frequency domain (FD) LFT formulation. In Figure 11 the upper (UB) and lower (LB) μ bound results obtained with both approaches are shown. The observable matching can be considered a validation of the implemented processes.

The estimation given by the algorithms is very accurate since the values of the bounds are in close agreement, meaning that the actual value of μ is well predicted. In particular it can be concluded from this plot that the system is flutter free for structural uncertainties up to approximately 70% ($\approx \frac{1}{1.4}$) of the assumed size. Robust analysis carried out by means of s.s.v., since it is inherently a frequency domain technique, gathers also a frequency perspective on the uncertainty-prompted instability onset. This is an important feature enriching the content of the prediction with something more than a simple binomial-type of output (either the system is robustly stable or not within the defined uncertainty set). In particular it shows the peak frequency at which instability occurs, how much it is modified compared to the nominal case, and when multiple instabilities exist it also

provides insight into the different mechanisms taking place. In this example, the peak frequency is at about ω_P=72.2$\frac{rad}{s}$. This frequency is slightly greater than the nominal flutter frequency ω_f=70.7$\frac{rad}{s}$ shown in Figure 10. This change can probably be ascribed to the modified values in the structural parameters and to a different wind speed (270$\frac{m}{s}$ instead of the flutter speed 303$\frac{m}{s}$) which causes a different aerodynamic contribution to the system's frequencies. As can be observed in Figure 10, pitch frequency (responsible for the instability) is indeed higher at lower speeds than at V_f.
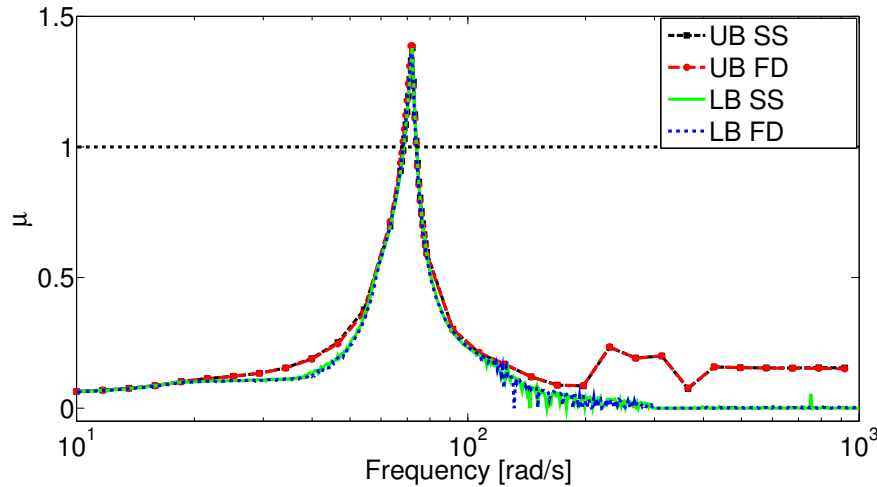
Figure 11. μ bounds for the case of structural uncertainties in inertia and stiffness. A comparison between the state-space (SS) and frequency domain (FD) formulation

Due to the accurate estimation of the lower bound, it is possible to extract the smallest perturbation matrix $\boldsymbol{\Delta_S}^{cr}$ capable of causing instability, corresponding to the peak in the graph of Figure 11:

$$
\begin{aligned}
\boldsymbol{\Delta_S}^{cr} &= \mathrm{diag}(\delta_{Ms11}^{cr}, \delta_{Ms12}^{cr}I_2, \delta_{Ms22}^{cr}, \delta_{Ks11}^{cr}, \delta_{Ks22}^{cr}) \\
&= \mathrm{diag}(-0.7245, 0.7245I_2, 0.711, 0.6460, -0.7213)
\end{aligned}
\tag{37}
$$

To further highlight the completeness of analysis that μ allows when reconciled with adequate system understanding, an interesting interpretation of the worst parameter combination reported in (37) is described. From examining the signs and values of the above worst-combination it is noted that the structural parameters have opposite perturbations if grouped according to the affected degrees of freedom (matrix subscripts 11 for the plunge, and 22 for the pitch). Specifically, the plunge equilibrium sees a reduction in M_{s11} and an increase in K_{s11}, while the pitch equilibrium sees an increase in M_{s22} and a reduction in K_{s22}. From a free-vibration analysis point of view, this corresponds to getting the plunge and pitch natural frequencies closer, which is a trend known to be detrimental to flutter stability. Thus, μ analysis was capable not only of predicting quantitatively the reduction of stability margin in view of the uncertainty set, but also to point out the mechanism underlying the worst-case flutter onset. This kind of *supplementary* information may be in general of great utility to inform design actions or sketch out robust control strategies for flutter suppression. It is highlighted that this μ-based system insight is only possible when reconciling both understanding of μ analysis capabilities and of the system behavior (in this case, flutter).

The study of this case is concluded with Figure 12 which shows the time-response of the system (for clarity only the plunge displacement is depicted) at V=270 $\frac{m}{s}$ for two perturbation matrices. In the first case the uncertain structural parameters are modified according to the matrix $\boldsymbol{\Delta_S}^{cr}$ in

(37) obtained from the μ lower bound of Figure 11. In the second case, this perturbation matrix is uniformly scaled by a factor of 0.99. The two responses showcase the ability of μ in detecting exactly the worst-case instability, since a slightly smaller perturbation proves to be unable to drive the system unstable.
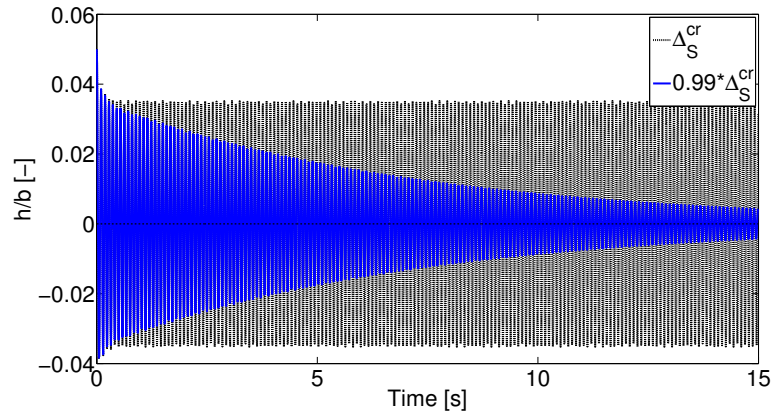

Figure 12. Time-response of the plunge DOF for two different perturbation matrices

The above interpretations are based on the tightness of the bounds: if the gap is large only conservative conclusions can be made on the system robustness. In the next subsection numerical aspects related to the usage of μ analysis for robust flutter calculations are discussed.

5.3. Aerodynamic uncertainty analysis

The RS of the system when the aerodynamics part is also affected by uncertainties is now addressed. The considerations about LFT modeling and uncertainty description discussed respectively in Subsections 4.1 and 4.2 are the foundation for what is shown now.

For the first analysis, the system is recast in the framework suitable for μ analysis through the process described in Section 4.1.1 and the uncertainty block $\mathbf{\Delta_T}$ defined in (29) is considered. This is equivalent to assuming uncertainty in the three transfer functions $A_{T_{12}}$, $A_{T_{21}}$ and $A_{T_{22}}$ of the AIC matrix given by the Theodorsen theory. They range in the disc of the complex plane centered in the nominal values and have radii equal to 10% of their magnitudes. In this case the uncertainty description consists of only three non-repeated complex uncertainties and the calculation of μ is now exacts as visible in the perfect overlapping of the two graphs in Figure 13. This is a known property of the s.s.v. computation in the presence of pure complex uncertainties [36].

It follows a discussion of the predictions attained when the plant is formulated in state-space, in particular we consider uncertainties in the lag roots of the unsteady part of the approximation only. The *aerodynamic* LFTs $\mathcal{F}_u(\hat{\mathbf{A}}, \mathbf{\Delta})$ corresponding to this uncertainty description were defined in (30). Based on the knowledge of the nominal flutter frequency corresponding to a reduced flutter frequency $k_f \cong 0.3$: for the Roger approximation four aerodynamic roots equally spaced between -0.2 and -0.6 are selected (yielding a state-matrix of dimension 18), while for the MS method five aerodynamic roots equally spaced in the same range are used (state-matrix dimension of 11). The LFT coverage in Figure 8 and all the related comments suggest that when these two uncertainty descriptions hold the same allowed range of variation (here fixed at 10%) they produce very different
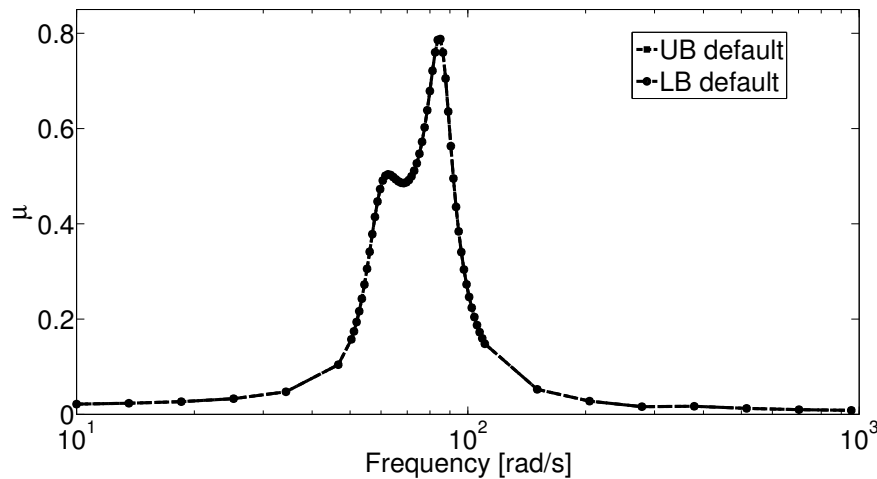
Figure 13. μ bounds for the case of aerodynamic uncertainties in the Theodorsen aerodynamics operator

frequency response families and consequently robust stability margins. In an attempt to reconcile the maps defined by (30), in Subsection 4.2 it was proposed to scale the uncertainty levels of one of the two sets in order to equalise the H_∞ norm of the uncertain aerodynamic transfer matrices. Figure 14 shows the results considering the same level of uncertainty and that obtained by applying a scaling of the range of variation for the lag roots in the Minimum State approximation in accordance with the aforementioned criterion. It is evident that the predictions in the first case are far apart, whereas with this pre-scaling the difference in the peak value falls below 30%. It is restated here that this criterion does not allow the two uncertainty definitions to be reconciled exactly, due to the inherent differences in the definition of $\mathbf{\Gamma}_{lag-Roger}$ and $\mathbf{\Gamma}_{lag-MS}$ (see Equations (14) and (17) respectively), but it is thought as a useful device to define consistent uncertainty levels when the two different approximations are employed, and in general to inform the selection of the amount of uncertainty held in the LFT in order to reduplicate a given data dispersion.
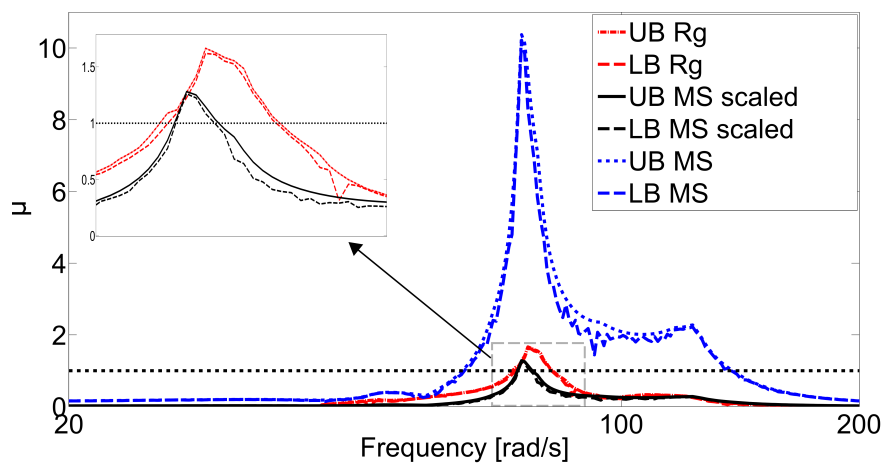

Figure 14. Comparison of μ bounds for the case of uncertainties in the lag roots of the two approximated aerodynamic operators (considering both scaled and same uncertainty level in $\mathbf{\Delta}_{\mathbf{MS-L}}$)

5.4. Full (structural and aerodynamic) uncertainty analysis

Finally, as a validation of the unifying approach for the aerodynamic uncertainty description presented in Subsection 4.2.2, Figure 15 shows a comparison of μ calculation (for clarity only μ_{UB} is reported) considering the complete scenario featuring uncertainties in both the structural (mass and stiffness matrices) and aerodynamic part of the model. The uncertainty description, resulting in a mixed real-complex $\mathbf{\Delta}$ matrix, is a compound of two separate cases investigated earlier and is summarised as follows:

$$
\begin{aligned}
\mathbf{\Delta}^{6,R-3,C} &= \mathrm{diag}(\mathbf{\Delta_S}^{6,R}, \mathbf{\Delta_T}^{3,C}) \\
&= \mathrm{diag}(\delta_{Ms11}, \delta_{Ms12}I_2, \delta_{Ms22}, \delta_{Ks11}, \delta_{Ks22}, \delta_{A_{T_{12}}}, \delta_{A_{T_{21}}}, \delta_{A_{T_{22}}})
\end{aligned}
\tag{38}
$$

The frequency domain approach predictions (*FD*) are plotted against those obtained with the strategy proposed in this section (labelled *SS with FD*). The results almost perfectly match. In making a comparison it should also be kept in mind that the nominal plant is defined by two different models and thus this could generate a slight mismatch in the predictions.
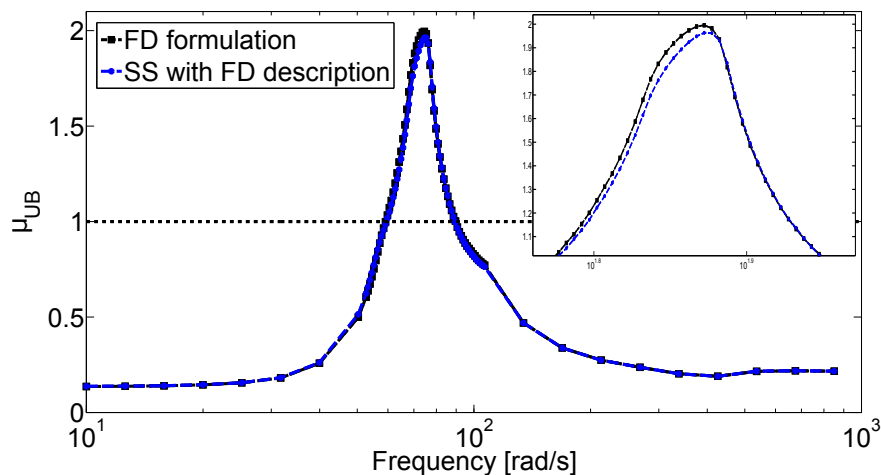

Figure 15. Comparison of μ upper bound for the case of aerodynamics and structural uncertainties adopting frequency domain and unified formulation

6. CONCLUSIONS

In this paper, the robust flutter stability problem has been investigated in its critical modeling and analysis aspects. An aeroelastic framework that is simple, but representative of modern applications, was selected and described in its essential features. Two different starting points for the LFT modeling process, related to the adoption of an unsteady aerodynamic operator, were identified. The different strategies enabling the problem to be recast for μ analysis applications were discussed, and a critical examination of aeroelastic uncertainty descriptions was presented.

This study complements existing works on the topic, in that on the one hand it reviews in detail the possible approaches highlighting the connections between modeling choices and robustness results. And on the other hand, it shows a new angle on the differences in handling aerodynamic uncertainties, known to play a crucial role in obtaining profitable flutter predictions. In this regard, a new approach is proposed which allows a physical-based uncertainty description of the unsteady

aerodynamic operator to be provided; this also makes the μ computation a mixed real-complex problem when the system is described by means of a state-space model, as in robust control practice.

It is thus believed that these discussions can help to get a better insight into the robust-oriented aeroelastic modeling task and can provide in general guidance on the application of the LFT-μ paradigm to address robustness. It is highlighted that in this article a detailed presentation approach (if at times tending to be basic for either the μ analysis or the aeroelastic experts) has been favored in pursuit of establishing a common ground between the robust control and the aeroelastic communities –specifically in respect of robust modeling and analysis of flutter.

APPENDIX A   TYPICAL SECTION PARAMETERS

The parameter values for the analysed test case, taken from [26], are reported in Tab. II. Note that, according to these definitions, all the three equilibria in (8) are assumed to be written in Newton (N).

Table II. Parameters for the Typical Section model

Name	Value	Name	Value
b	1 m	r_α	0.497
a	-0.4	K_h	$3.85*10^5\ N$
c	0.6	K_α	$3.85*10^5\ N$
x_α	0.2	K_β	$8.66*10^4\ N$
m_s	$153.94\ \frac{kg}{m}$	c_h	$0\ Ns$
r_β	0.0791	c_α	$0\ Ns$
S	$2*b^2$	c_β	$0\ Ns$
x_β	-0.025	ρ	$1.225\ \frac{kg}{m^3}$

As for the aerodynamic model, the Theodorsen AIC matrix $\mathbf{A}(\bar{s})$ was presented in (10). The real coefficient matrices $\mathbf{M_{nc}}$, $\mathbf{B_{nc}}$, $\mathbf{K_{nc}}$, $\mathbf{RS_1}$ and $\mathbf{RS_2}$, representing respectively inertial, damping and stiffness noncirculatory terms and damping and stiffness circulatory terms, depend on the dimensionless distances a and c. Their analytical expressions is omitted here for space constraints and can be found in [22].

$C(\bar{s})$ is the Theodorsen function, which is a complex scalar defined as:

$$C(\bar{s}) = \frac{K_1(\bar{s})}{K_0(\bar{s}) + K_1(\bar{s})} = \frac{H_1(z)}{H_1(z) + iH_0(z)}; \qquad z = -i\bar{s} \tag{39}$$

where K_n and H_n are respectively modified Bessel functions and Hankel functions of order n. The former can be obtained, at a given reduced frequency k, with the MATLAB function *besselh*.

REFERENCES

1. Hodges DH, Pierce GA. *Introduction to Structural Dynamics and Aeroelasticity*. Cambridge University Press, 2011.
2. Pettit CL. Uncertainty Quantification in Aeroelasticity: Recent Results and Research Challenges. *Journal of Aircraft* 2004; **41**(5):1217–1229.
3. Zhou K, Doyle JC, Glover K. *Robust and Optimal Control*. Prentice-Hall, Inc., 1996.
4. Doyle J. Analysis of feedback systems with structured uncertainties. *IEE Proceedings D Control Theory and Applications* 1982; **129**(6):242–250.
5. Lind, R and Brenner, M. *Robust Aeroservoelastic Stability Analysis*. Advances in Industrial Control, Springer, 2012.
6. Borglund D. The μ-k Method for Robust Flutter Solutions. *Journal of Aircraft* 2004; **41**(5):1209–1216.

7. Karpel M, Moulin B, Idan M. Robust Aeroservoelastic Design with Structural Variations and Modeling Uncertainties. *Journal of Aircraft* 2003; **40**(5):946–952.

8. Lind R, Brenner M. Flutterometer: An On-Line Tool to Predict Robust Flutter Margins. *Journal of Aircraft* 2000; **37**(6):1105–1112.

9. Marcos A, Balas G. Development of Linear Parameter Varying Models for Aircraft. *J. of Guidance, Control and Dynamics* 2004; **27**(2):218–228.

10. Marcos A, Bennani S, Roux C, Valli M. LPV modeling and LFT Uncertainty Identification for Robust Analysis: application to the VEGA Launcher during Atmospheric Phase. 1st IFAC Workshop on Linear Parameter Varying Systems, 2015.

11. Magni J. Linear fractional representation toolbox modelling, order reduction, gain scheduling. *Technical Report TR 6/08162*, DCSD, ONERA, Systems Control and Flight Dynamics Department 2004.

12. Iannelli A, Marcos A, Lowenberg M. Comparison of Aeroelastic Modeling and Robust Flutter Analysis of a Typical Section. IFAC Symposium on Automatic Control in Aerospace, 2016.

13. Bisplinghoff RL, Ashley H. *Principles of Aeroelasticity*. Wiley, 1962.

14. Shin J, Balas G, Packard A. Worst-Case Analysis of the X-38 Crew Return Vehicle Flight Control System. *J. of Guidance, Control and Dynamics* 2001; **24**(2):261–269.

15. Poussot-Vassal C, Roos C. Generation of a reduced-order LPV/LFT model from a set of large-scale MIMO LTI flexible aircraft models. *Control Engineering Practice* 2012; **20**(9):919–930.

16. Ferreres G, Fromion V, Duc G, M'Saad M. Application of real/mixed μ computational techniques to an H_∞ missile autopilot. *International Journal of Robust and Nonlinear Control* 1996; **6**(8):743–769.

17. Mannchen T, Bates D, Postlethwaite. Modeling and Computing Worst-Case Uncertainty Combinations for Flight Control Systems Analysis. *J. of Guidance, Control and Dynamics* 2002; **Vol. 25**(No. 6):pp. 1029–1039.

18. Simplicio P, Bennani S, Marcos A, Roux C, Lefort X. Structured Singular-Value Analysis of the Vega Launcher in Atmospheric Flight. *J. of Guidance, Control and Dynamics* 2016; **Vol. 39**(No. 6):pp. 1342–1355.

19. Marcos A, Bates D, Postlethwaite I. A symbolic matrix decomposition algorithm for reduced order linear fractional transformation modelling. *Automatica* 2007; **43**(7):1211 – 1218.

20. Belcastro C. On the numerical formulation of parametric linear fractional trasnformations (LFT) uncertainty models for multivariate matrix polynomial problems. *Technical Report NASA/TM-1998-206939* 1998.

21. Braatz R, Young P, Doyle J, Morari M. Computational-complexity of μ-calculation. *IEEE Transactions on Automatic Control* 1994; **39**(5):1000–1002.

22. Theodorsen T. General Theory of Aerodynamic Instability and the Mechanism of flutter. *Naca Report 496* 1935; .

23. Albano E, Rodden W. A doublet lattice method for calculating lift distributions on oscillating surfaces in subsonic flows. *AIAA Journal* 1968; **7**(2):279–285.

24. Rodden WP, Johnson EH. *User Guide V 68 MSC/NASTRAN Aeroelastic Analysis*. MacNeal-Schwendler Corporation, 1994.

25. Roger K. Airplane Math Modeling Methods for Active Control Design. *AGARD-CP-228* 1977; .

26. Karpel M. Design for Active and Passive Flutter Suppression and Gust alleviation. *Nasa Report 3482* 1981.

27. Idan M, Karpel M, Moulin B. Aeroservoelastic Interaction Between Aircraft Structural and Control Design Schemes. *J. of Guidance, Control and Dynamics* 1999; **22**(4):513–519.

28. Doyle J, Packard A, Zhou K. Review of LFTs, LMIs, and μ. IEEE Conference on Decision and Control, 1991.

29. Varga A, Looye G. Symbolic and numerical software tools for lft-based low order uncertainty modeling. Proc. of the IEEE International Symposium on Computed Aided Control System Design, 1999.

30. Roos C, Hardier G, Biannic JM. Polynomial and rational approximation with the APRICOT library of the SMAC toolbox. Proceedings of the IEEE Multiconference on Systems and Control, 2014.

31. Heinze S, Borglund D. Robust Flutter Analysis Considering Mode Shape Variations. *Journal of Aircraft* 2008; **45**(3):1070–1074.

32. Kumar A, Balas G. An approach to model validation in the μ framework. American Control Conference, 1994.

33. Balas G, Chiang R, Packard A, Safonov M. *Robust Control Toolbox*. 2009.

34. Theis J, Pfifer H, Seiler P. Robust Control Design for Active Flutter Suppression. AIAA SciTech Forum, 2016.

35. Hassig HJ. An approximate true damping solution of the flutter equation by determinant iteration. *Journal of Aircraft* 1971; **Vol. 33**(7):885–889.

36. Packard A, Doyle J. The Complex Structured Singular Value. *Automatica* 1993; **29**(1):pp. 71–109.